Available online at www.sciencedirect.com
SCIENCE DIRECT
Lithos 89 (2006) 353–376
LITHOS
www.elsevier.com/locate/lithos

The Fedorivka layered intrusion (Korosten Pluton, Ukraine): An example of highly differentiated ferrobasaltic evolution

J.C. Duchesne [a,*], L. Shumlyanskyy [b], B. Charlier [a]

[a] *Department of Geology, University of Liège, Bat. B20, B-4000 Sart Tilman, Belgium*
[b] *Institute of Geochemistry, Mineralogy and Ore formation of the National Academy of Sciences of Ukraine, KYIV 01001, Ukraine*

Received 24 June 2005; accepted 9 January 2006
Available online 31 March 2006

Abstract

This study documents the petrography and whole-rock major and trace element geochemistry of 38 samples mainly from a drill core through the entire Fedorivka layered intrusion (Korosten Pluton), as well as mineral compositions (microprobe analyses and separated mineral fraction analyses of plagioclase, ilmenite, magnetite and apatite) of 10 samples. The Fedorivka layered intrusion can be divided into 4 lithostratigraphic units: a Lower Zone (LZ, 72 m thick), a Main Zone (MZ, 160 m thick), and an Upper Border Zone, itself subdivided into 2 sub-zones (UBZ_2, 40 m thick; UBZ_1, 50 m thick). Igneous lamination defines the cumulate texture, but primary cumulus minerals have been affected by trapped liquid crystallization and subsolidus recrystallization. The dominant cumulus assemblage in MZ and UBZ_2 is andesine (An_{39-42}), iron-rich olivine (Fo_{32-42}), augite ($En_{29-35}Fs_{24-29}Wo_{42-44}$), ilmenite ($Hem_{1-6}$), Ti-magnetite ($Usp_{52-78}$), and apatite. The data reveal a continuous evolution from the floor of the intrusion (LZ) to the top of MZ, due to fractional crystallization, and an inverse evolution in UBZ, resulting from crystallization downwards from the roof. The whole-rock Fe/Mg ratio and incompatible element contents (e.g. Rb, Nb, Zr, REE) increase in the fractionating magma, whereas compatible elements (e.g. V, Cr) steadily decrease. The intercumulus melt remained trapped in the UBZ cumulates due to rapid cooling and lack of compaction, and cumulus mineral compositions re-equilibrated (e.g. olivine, Fe–Ti oxides). In LZ, the intercumulus melt was able to partially or totally escape. The major element composition of the MZ cumulates can be approximated by a mixing (linear) relationship between a plagioclase pole and a mafic pole, the latter being made up of all mafic minerals in (nearly) constant relative proportions. By analogy with the ferrobasaltic/jotunitic liquid line of descent, defined in Rogaland, S. Norway, and its conjugated cumulates occurring in the Transition Zone of the Bjerkreim-Sokndal intrusion (Rogaland, a monzonitic (57% SiO_2) melt is inferred to be in equilibrium with the MZ cumulates. The conjugated cumulate composition falls (within error) on the locus of cotectic compositions fixed by the 2-pole linear relationship. Ulvöspinel is the only Ti phase in some magnetites that have been protected from oxidation. QUIlF equilibria in these samples show that magnetite and olivine in MZ have retained their liquidus compositions during subsolidus cooling. This permits calculation of liquidus fO_2 conditions, which vary during fractionation from $\Delta FMQ = 0.7$ to -1.4 log units. Low fO_2 values are also evidenced by the late appearance of cumulus magnetite (Fo_{42}) and the high V^{3+}-content of the melt, reflected in the high V-content of the first liquidus magnetite (up to 1.85% V).

Keywords: Ferrobasalt; Anorthosite; Jotunite; Fe–Ti oxide minerals; Vanadium; Layered intrusions

* Corresponding author. Tel.: +32 43 66 2255; fax: +32 43 66 2921.
E-mail address: jc.duchesne@ulg.ac.be (J.C. Duchesne).

0024-4937/$ - see front matter © 2006 Elsevier B.V. All rights reserved.
doi:10.1016/j.lithos.2006.01.003

1. Introduction

Layered intrusions have played an important role in the understanding of igneous rocks and their processes of formation. They have allowed determination of the properties of cumulates and their mechanisms of formation. They have also permitted to define several characteristic cumulate series which mirror the evolution of magmatic melts. In particular, the determination of the *P*, *T* and oxygen fugacity (fO_2) controlling their evolution has been a major step in deciphering the diversity of liquid lines of descent. The study of layered intrusions has also revealed the complexity of the physical and chemical processes occurring during the lifetime of magma chambers in possible connection with volcanic phenomena.

Since the pioneering work of Wager, it has become increasingly obvious that individual layered intrusions (see the reviews of Wager and Brown, 1968; Parsons, 1987; Cawthorn, 1996) are unique in many ways because some of their features result from a specific combination of controlling factors, such as *T*, *P*, fO_2, nature of magma and cooling regime. Each layered intrusion thus represents a natural laboratory where theoretical models can be confronted and tested against observations.

Here we document the Fedorivka layered intrusion (FLI), that is part of the Korosten Pluton. The interest is three-fold. Firstly, the rocks belong to the ferrobasalt family. Experimental data have recently been presented on this type of magma that document the role of fO_2 on the differentiation process (Snyder et al., 1993; Toplis and Carroll, 1994; Toplis et al., 1994a,b; Toplis and Corgne, 2002). Secondly, the FLI is emplaced in an andesine anorthosite-rapakivi plutonic complex, the Korosten Pluton, which contains a typical AMCG suite of rocks (Anorthosite–Mangerite–Charnockite–(rapakivi) Granite). In the anorthosite literature, the FLI would be considered as related to ferrodiorites (Ashwal, 1993), monzonorites (Duchesne et al., 1989; Duchesne, 1990) or, preferably, jotunites (i.e. Fe–Ti–P-rich hypersthene monzodiorites) (Vander Auwera et al., 1998b). Jotunitic melts, whether they are residual melts from anorthosite fractionation (e.g. Morse, 1982; Emslie, 1985; Wiebe, 1992; Scoates et al., 1996) or a direct product of gabbronorite melting (e.g. Taylor et al., 1984; Duchesne et al., 1999; Longhi et al., 1999; Longhi, 2005), lead through fractional crystallization to silica-enriched magmas rather than to melts highly enriched in Fe (Duchesne, 1990; Owens et al., 1993; Vander Auwera et al., 1998b). They can therefore shed some light on the still debated nature of the Skaergaard differentiated melts (Hunter and Sparks, 1987; Duchesne, 1990; McBirney and Naslund, 1990; Morse, 1990). We will present evidence pointing to the silica-enriched nature of the melt in equilibrium with the most evolved FLI cumulates. Thirdly, the FLI has been considered as a potentially economic Fe–Ti–V–P deposit (Gursky et al., 2003) and was explored accordingly. We show that the average composition of the mafic cumulates contains 9.8% $TiO_2+P_2O_5$, but that the maximum enrichment is 9% TiO_2 and 4.6% P_2O_5. Vanadium contents are high (up to 1.85% V in magnetite) due to low fO_2 during crystallization.

Since there are similarities in the mineral assemblages, we will frequently refer to the Skaergaard intrusion (see the review in McBirney, 1996) and to the Bjerkreim-Sokndal layered intrusion in the Rogaland anorthositic province (Wilson et al., 1996; Duchesne and Korneliussen, 2003).

2. The Korosten anorthosite–rapakivi granite Pluton: an overview

The Korosten anorthosite–rapakivi granite Pluton (Fig. 1) occupies about 12 000 km^2 within the northwestern region of the Ukrainian shield, and is one of several large Proterozoic massifs that intrude the basement of the East-European craton. It is hosted by the amphibolite facies metamorphic rocks of the Teteriv series and by the orogenic granites of the Zhitomir and Osnitsk complexes (Skobelev, 1987). Its emplacement spanned a long time interval, from 1800 to 1737 Ma, although the majority of mafic rocks intruded in a rather short period at 1767–1758 Ma (see Bogdanova et al., 2004 for a review).

Anorthosite and related mafic rocks occupy about 18% of the Korosten Pluton. They occur in three large bodies, the Volodarsk-Volynskyy, the Chopovichi and the Fedorivka massifs (Fig. 1), the rest being represented by rocks of rapakivi granite affinity (Bogdanova et al., 2004). Detailed field investigations carried out by Mitrokhin (2003) and age determinations (Amelin et al., 1994; Verkhogliad, 1995) suggest that anorthosites and related mafic rocks were emplaced in a series of events. This led to a complex internal pattern made up of several rock suites: (1) the *early anorthosite suite* (A_1; 1800 to 1784 Ma) is represented by xenoliths in younger rocks. The rocks, made up of aggregates of giant plagioclases and high-Al orthopyroxenes, are the most primitive in terms of Sr-isotope composition; (2) the *main anorthosite suite* (A_2; 1760–1758 Ma), including the typical black, coarse-grained anorthosite, with zoned iridescent plagioclase, inverted pigeonite, augite and

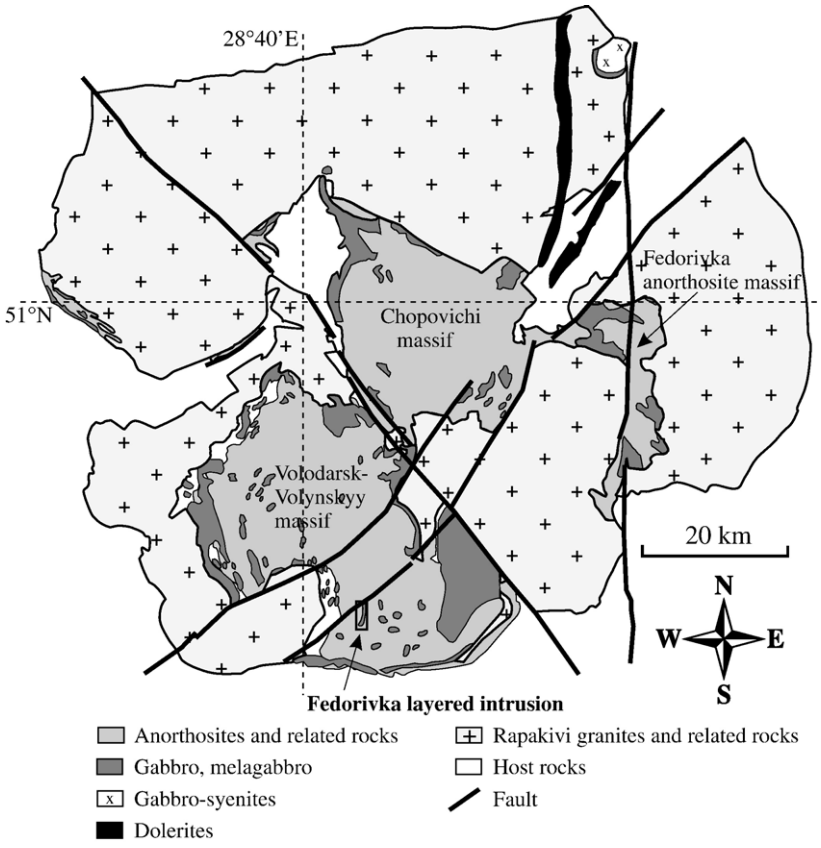

Fig. 1. Geological map of the Korosten Pluton (after Shcherbak et al., 1984). The recent sediment cover has been removed.

iron-rich olivine, which occurs in e.g. the Volodarsk-Volinskyy massif; (3) the *early gabbroic suite* (G_3) and the *late gabbroic suite* (G_4; 1759 Ma) are represented by numerous intrusions within the A_2 anorthosites and along their margins (Fig. 1); G_4 gabbros are olivine-bearing gabbro-dioritic rocks with relatively high abundances of ilmenite, magnetite and apatite; (4) finally, the *dyke suite* (D_5), comprising dolerite, trachybasalt and trachyandesite, cutting across the anorthosite massifs, rapakivi granites and surrounding rocks.

3. The Fedorivka olivine gabbro layered intrusion

The Fedorivka olivine gabbro layered intrusion (FLI)–not to be confused with the Fedorivka anorthosite massif (Fig. 1)–belongs to the G_4 rock suite and is located in the southern part of Volodarsk-Volynskyy massif (Fig. 1). It is entirely covered by recent deposits but has been explored by numerous boreholes. This study is based on samples from 6 drill cores (579–585) along AB, supplemented by drill core 599 (Fig. 2).

In plan view the FLI is "banana-shaped", elongated in a NE–SW direction. It can be traced along strike over ca. 3.5 km, and its width does not exceed ca. 450 m (Fig. 2A). Based on drill cores (Prykhodko et al., 2002), the FLI in vertical cross-section is a trough-shaped body (Fig. 2B). The maximal vertical thickness of the body is 320 m. Contacts with the host Volodarsk-Volynskyy anorthosite and leucogabbro are sharp and intrusive. Large xenoliths of host rocks up to several meters across are common near the contacts in the drill cores. The northern portion of the intrusion was studied in much less detail than the southern part, and only the latter, regarded as a sub-economic ilmenite–apatite deposit, will be dealt with here.

In the enclosing anorthosites of the Volodarsk-Volynskyy massif plagioclase (1 to 5 cm; higher than 90 modal %) forms a network of tabular, euhedral, unzoned crystals, between which are mafic minerals (iron-rich olivine (ca. Fo_{44}), augite and inverted pigeonite). Minor phases are opaques, quartz, biotite, and apatite.

In contrast with the enclosing anorthosite, the FLI rocks are medium-grained, equigranular, with a grain size between 0.4 and 1 mm. They are rather homogeneous with respect to their textures but have variable

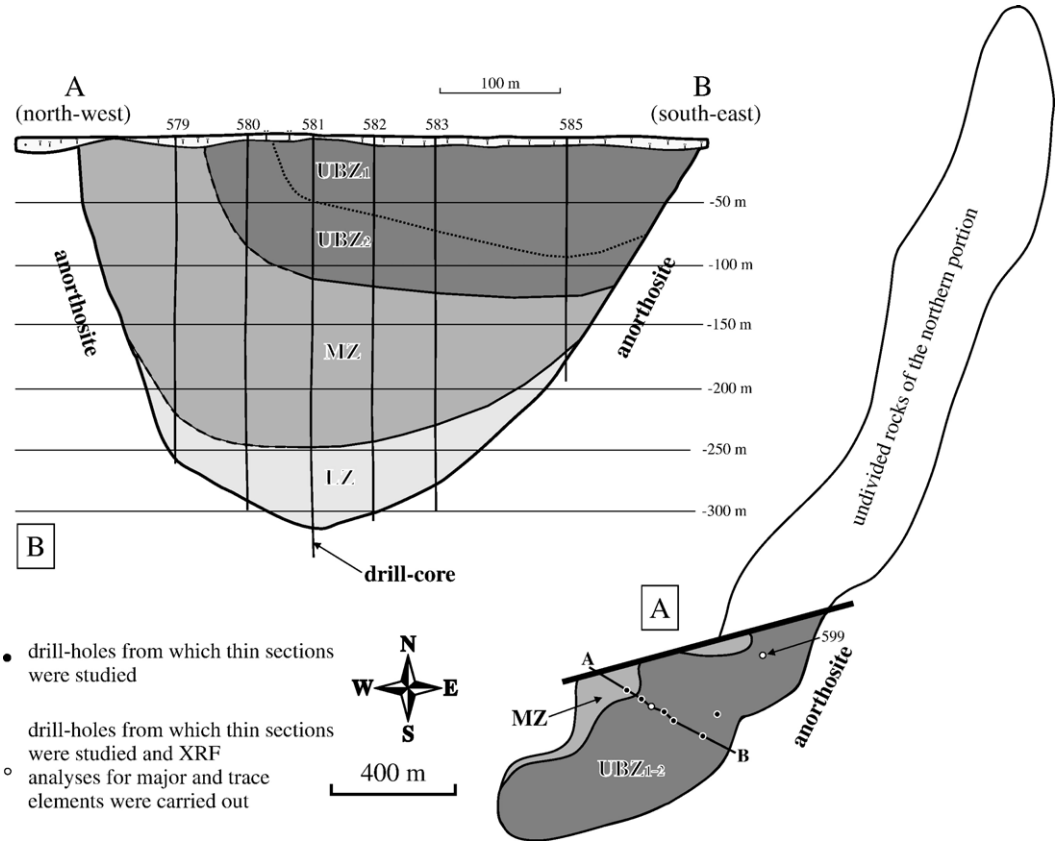

Fig. 2. (A) Schematic geological map of the Fedorivka layered intrusion with position of the AB section and studied drill cores. (B) Cross section through the Fedorivka layered intrusion along profile AB showing location of the six drill cores. The subdivision into stratigraphic zones, based on data from borehole 581, has been extended to the whole section on the basis of the petrographic study of thin sections.

colour index. The main rock-forming minerals are andesine, iron-rich olivine, augite, ilmenite, Ti-magnetite, apatite and small amounts of biotite. Ca-poor pyroxene is lacking. Two main rock types can be distinguished: meso- to melanocratic oxide-rich olivine gabbro (the potential apatite–ilmenite ore), and more leucocratic gabbro that forms thin layers within the thick melanocratic horizons, or thicker leucocratic units in the upper and lower parts of the intrusion.

3.1. Petrography

Plagioclase normally forms ca. 1 mm-sized tabular grains, but is somewhat coarser in the lower part of the intrusion. Single plagioclase grains with high aspect ratio and larger dimensions (up to 6 mm) (Fig. 3C, D) occur locally in all rock types. Some plagioclase crystals are slightly deformed (bent, kinked or granulated), possibly due to compaction. Olivine appears as equant or slightly elongated oval grains. Clinopyroxene (augite) is sub- to euhedral. It contains numerous, small, regularly oriented plates of hematite (Schiller inclusions), that are more abundant in the cores of the grains than in the margins; this may be evidence of postcumulus overgrowths. Opaque minerals (ilmenite, Ti-magnetite, traces of sulphides) occur as equant or oval-shaped grains and occupy the interstitial space between the major silicates. They are locally rimmed by red-brown biotite. Sulphides (pyrrhotite, pyrite, small amounts of chalcopyrite) may locally form spherical grains. Apatite occurs as prismatic crystals, aligned parallel to the mineral lamination and varying in length from 0.5 to 1 mm. Smaller apatite crystals (50 to 70 μm) can also form inclusions in all other minerals, particularly in the marginal parts (Fig. 3C, D).

Although the minerals, and particularly plagioclase, appear optically homogeneous, microprobe investigations reveal a slight reverse zoning: at the rim, plagioclase is richer by 3–4% An, olivine by 1–4% Fo, augite by 1–2% En, than the core composition. This zoning, limited to the rim of the grains, has not

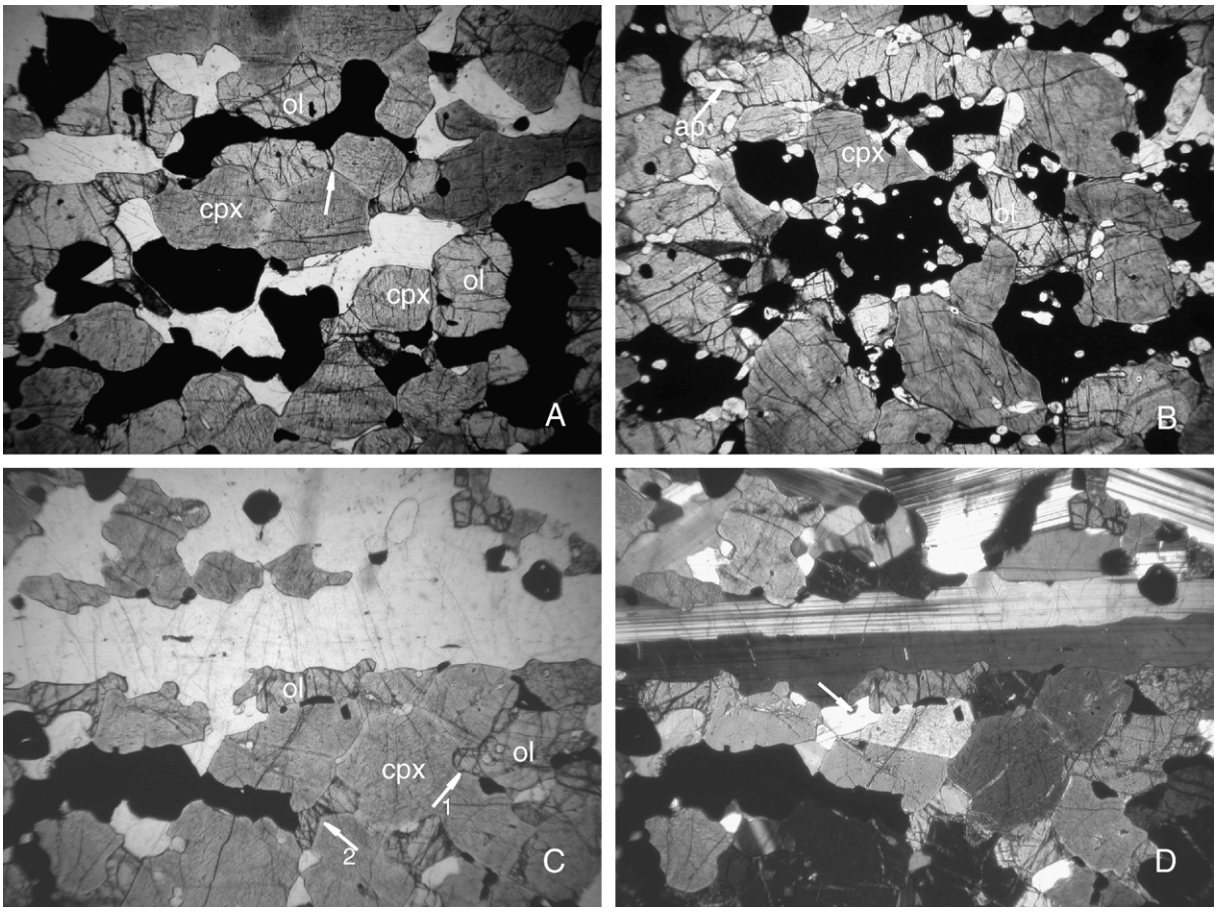

Fig. 3. (A) LZ olivine gabbro (581/274). The igneous lamination is defined by the elongation of the plagioclase, olivine, augite and ilmenite grains. Note the interstitial habit of the ilmenite, and close to the center (arrow), a triple junction between an olivine grain and two augite grains (with Schiller inclusion free rims). Plane polarized light. The long side of the photo is 5 mm. (B) UBZ_2 olivine melagabbro (581/73). Igneous lamination defined by olivine and augite grains (top of photo), as well as by opaque aggregates. A relatively large apatite prism (arrow) is elongated parallel to the lamination. Smaller apatites (intercumulus growth) are dispersed in the marginal portion of oxide minerals. Plane polarized light. Long side of the photo is 5 mm. (C) LZ olivine gabbro (581/277). A high aspect ratio plagioclase (>5 mm) defines lamination. Olivine can be wrapped by augite (arrow 1) or have an interstitial habit relative to augite grains (arrow 2). Triple junctions are common between mafic grains. Plane polarized light. Long side of the photo is 5 mm. (D) Same view in cross-polarized light. The long plagioclase displays combines Carlsbad and albite twinning. Note its intergrown boundaries with impingements on neighbouring grains. Small apatite grain (arrow) close to a contact.

significantly modified the bulk composition of the minerals.

The FLI rocks are clearly characterized by cumulate textures on both mesoscopic and microscopic scales. Cm-scale layering marked by abrupt changes in the modal composition is not rare. Under the microscope mineral lamination is common and sometimes beautifully displayed (Fig. 3). Elongated plagioclases define the plane of layering (Fig. 3C, D). The lamination is also marked by slightly elliptical olivine grains, by prismatic augites and elongated apatites and by the overall shape of opaque mineral domains.

This preferred orientation of the minerals can be taken as strong evidence for the cumulate character of the rocks, whatever the mechanism responsible for the texture (Hunter, 1996; Vernon, 2004). The marginal portions of the various minerals, however, reflect more complex processes than those involved by simple accumulation. For example, Fig. 5E shows that the magnetite can be wrapped by ilmenite, and Fig. 4F displays the inverse relation. Similarly, olivine and augite are interlobated and show reciprocal relationships: olivine is interstitial to augite and vice versa (e.g. Fig. 3C, D). Intergrown boundaries (resembling jig-saw puzzle pieces) are also common between plagioclase and the other minerals. The boundaries are sinuous with impingements between neighbouring grains (Fig. 3C, D). Short apatite crystals (ca. 50

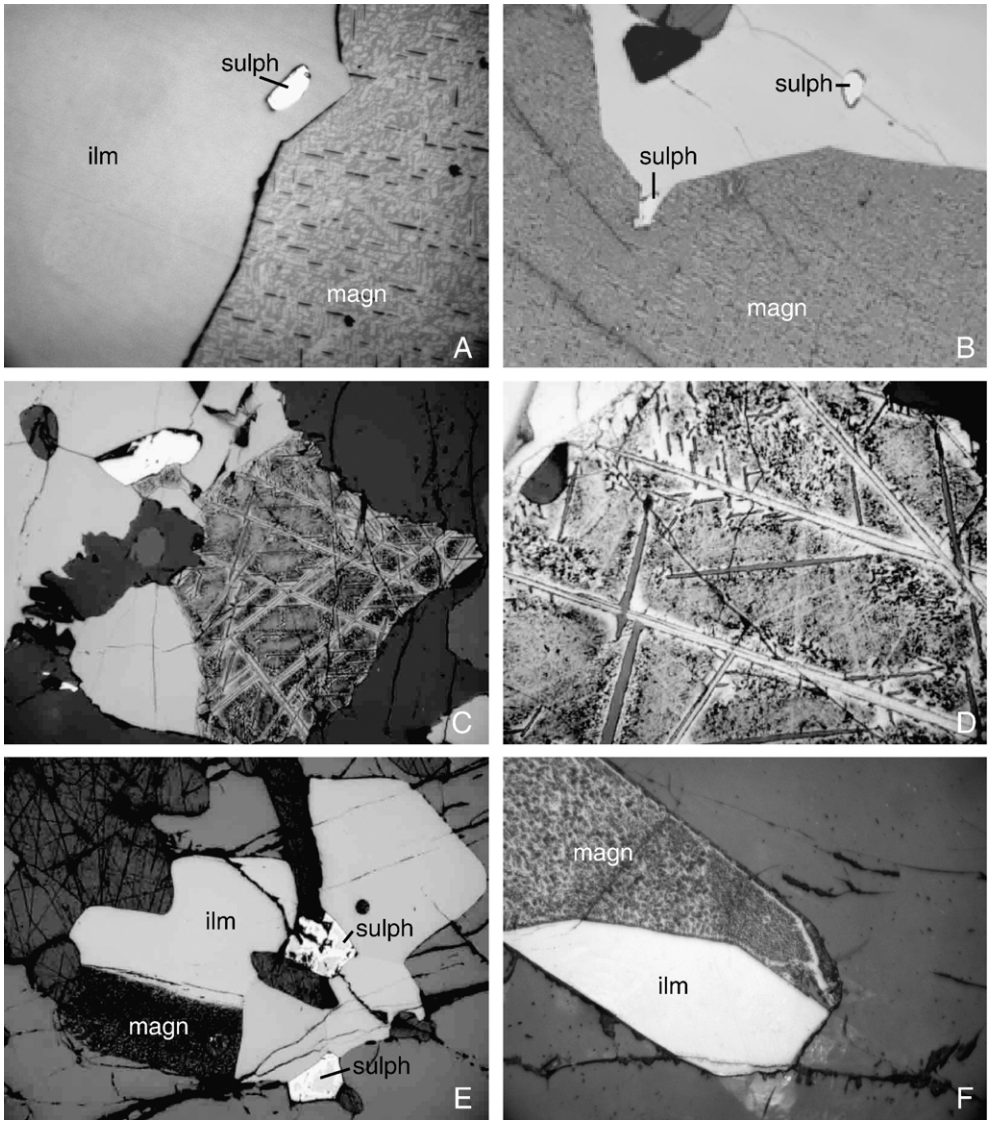

Fig. 4. (A) Light-grey (left) homogeneous ilmenite in contact with a cloth-textured magnetite (right) containing ulvöspinel (grey) and aluminous spinel (black) exsolutions in 100 planes of the host magnetite. A small grain of pyrite (sulph) occurs in the ilmenite grain. The contact is a broken straight line. The black line between the two oxides is a polishing artifact. MZ olivine gabbro (581/190b). Reflected light. The long side of the microphoto is about 0.3 mm. After etching with HCl. (B) A cloth-textured magnetite (magn) is in contact with an ilmenite containing two pyrite grains (sulph). The contact between the two oxides is a neat broken straight line. MZ olivine gabbro (581/190b). Long side of the microphoto is 0.6 mm. After etching with HCl. (C) Trellis-textured magnetite grain in contact with homogeneous ilmenite grains. The contact between the two oxides is irregular with a protrusion of magnetite in the ilmenite grain. The contacts between the oxides and silicates are notched and serrate. A sulphide grain is enclosed by ilmenite. LZ olivine gabbro (581/289). Reflected light, the long side of the microphoto is about 1.5 mm long. After etching with HCl. (D) Detail of (C). Etched trellis- and cloth-textured magnetite. A network of long ilmenite lamellae, along which clear zones of magnetite develop, in a cloth-textured magnetite (revealed by etching). Two sets (or generations) of aluminous spinel lamellae (grey) compete with the development of ilmenite lamellae. In the upper left corner, a thin rim of spinelliferous ilmenite is visible at the contact with the primary ilmenite grain. LZ olivine gabbro (581/289). Reflected light. Long side of the microphoto is about 0.3 mm. (E) A group of ilmenite grains, two sulphide grains and a cloth-textured (etched) magnetite grain. A prismatic apatite crystal is close to a sulphide. Note the texturally equilibrated contacts between all minerals and that the magnetite is wrapped by ilmenite, the opposite relationship to that observed in (B). Olivine gabbro from UBZ_1 (581/30). Long side of the microphoto is 1.5 mm. (F) Euhedral composite grain of ilmenite (light) intergrown with magnetite (grey). Ilmenite is clearly wrapped by magnetite and shows straight boundaries with it. The cloth texture of magnetite is revealed by HCl etching. MZ olivine gabbro (581/160a). Reflected light. The long side of the microphoto is about 1.5 mm.

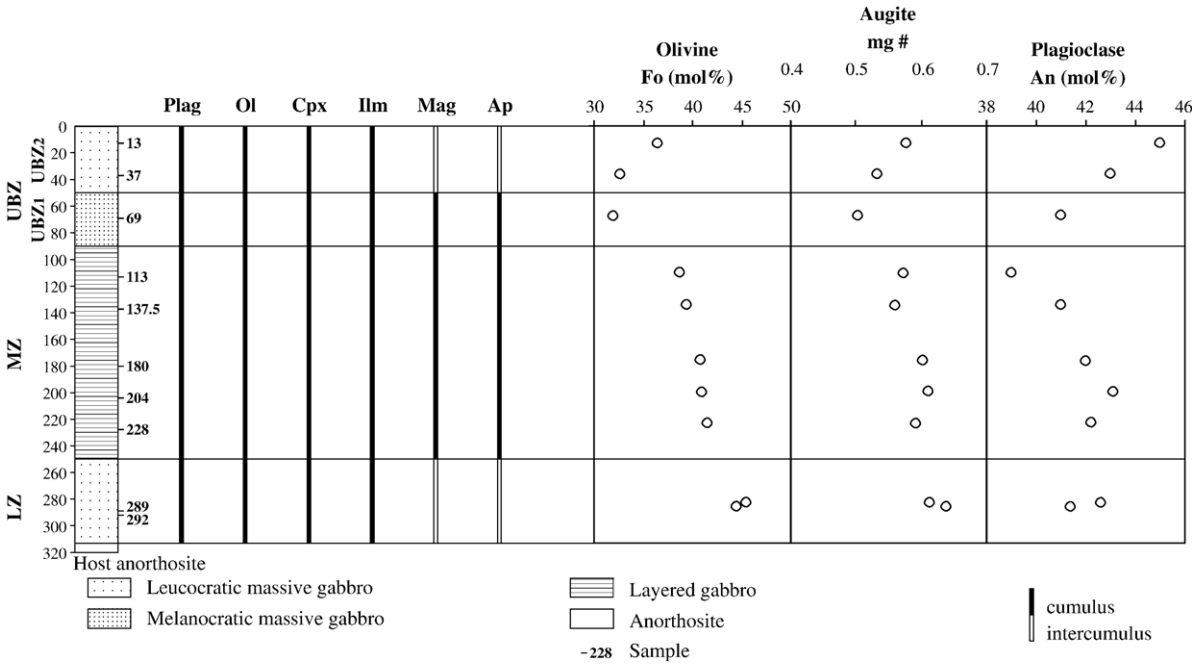

Fig. 5. Stratigraphic subdivision of the Fedorivka layered intrusion, major petrographic features, sample numbers from which minerals were analysed, as well as variation in olivine, augite and plagioclase compositions in drill core 581 (see on-line supplement Tables B1–B3 for analytical data).

μm long), much smaller than the cumulus apatites (Fig. 5C, D), are common in the border zones of the minerals or in the interstices between them. We interpret this second generation of apatite as having crystallized from trapped intercumulus liquid, together with the overgrowth material. These observations can be taken as evidence that the simple relationship between cumulus and intercumulus minerals is not the only factor controlling the observed textures. Subsolidus recrystallization (Hunter, 1996) has typically yielded readjusted grain boundaries (Fig. 4A,B,E,F), with the local development of texturally equilibrated contacts (e.g. Figs. 3A,D and 4E). Finally, as argued by Duchesne (1996, 1999), the interstitial habit of oxide minerals relative to the silicate minerals results from subsolidus recrystallization.

3.2. Fe–Ti oxide microtextures and compositional variations

Magnetite compositions in the FLI span a wide range of TiO_2 values, from 8.5% to 27.7% (Table 1), corresponding to recalculated ulvöspinel contents from 25% to 83%. This range of TiO_2 contents, which reaches remarkably high values, gives rise to a wide variety of microtextures visible under the microscope.

The most common type, found for high TiO_2 contents, is the *cloth microtexture* (Ramdohr, 1953): a very fine exsolution pattern of ulvöspinel lamellae (typically appearing like a closely woven piece of cloth) in the 100 planes of the magnetite host phase (Fig. 4A, B). This texture is easily revealed by brief etching of the polished surface with HCl. The dimension of the mesh is usually ca. 1–2 μm, but can go down to <1 μm (sample 69), in which case it is less easily etched and at the limit of microscopic observation. Small aluminous spinel lenses are also exsolved along the 100 planes (Fig. 4A,C,D). Ulvöspinel has been identified by X-ray diffraction (Fransolet, personal communication) in sample 69, where it appears as the only Ti-bearing component in the magnetite. This magnetite has thus not been oxidized at all. A similar ulvöspinel-magnetite cloth microtexture, with preservation of ulvöspinel, has been described in the Skaergaard intrusion (Vincent and Phillips, 1954; Vincent, 1960) and in the Fongen-Hyllingen intrusion (Thy, 1982). It is worth mentioning that, though cloth-textured titanomagnetites are common in gabbroic intrusions, they usually show subsolvus oxidation (e.g. Duchesne, 1972; Thy, 1982; Duchesne et al., 1987; Duchesne, 1999) without any ulvöspinel remaining.

A second type is the *trellis microtexture*: a network of ilmenite lamellae, parallel to 111 planes of the host magnetite (Fig. 4C,D), that results from an oxy-exsolution process. The ilmenite lamellae are locally thicker and can preferentially develop in a single plane, giving the *sandwich microtexture*. The trellis and

Table 1
Magnetite compositions from the Fedorivka intrusion determined by electron microprobe on cloth-textured grains (minimum and maximum values of TiO_2) and by XRF on separated fractions (average grain composition)

Sample/ depth	13	37			69			113			137.5			180			204			228			289
	XRF	EMP	EMP	XRF	EMP	EMP	XRF	EMP	EMP	XRF	EMP	EMP	XRF	EMP	EMP	XRF	EMP	EMP	XRF	EMP	EMP	XRF	XRF
SiO_2		0.03	0.05	0.56	0.03	0.04		0.03	0.04		0.06	0.02	0.54	0.04	0.06	0.68	0.11	0.09		0.05	0.09		
TiO_2	8.54	11.83	20.75	18.95	24.88	27.72	24.79	18.93	19.92	20.43	20.45	14.71	14.48	13.62	18.26	16.39	12.63	14.85	14.80	13.85	16.97	19.22	13.36
Al_2O_3		1.99	3.61	2.94	3.18	2.84		2.83	3.46		3.27	2.09	2.89	2.48	2.85	2.87	2.92	3.05		2.54	3.74		
Fe_2O_3	51.43	43.91	24.23		16.61	11.28		28.50	25.19		26.00	36.90		38.96	28.62		39.91	35.32		38.36	30.96		42.01
FeO	38.40	41.73	49.22		52.80	54.97		47.40	47.92		49.11	43.48		42.68	46.44		41.54	43.58		42.69	45.67		42.74
MnO	0.10	0.24	0.47	0.43	0.55	0.48	0.34	0.33	0.39	0.30	0.45	0.28	0.31	0.46	0.46	0.34	0.33	0.40	0.23	0.38	0.33	0.28	0.18
MgO		0.26	0.60	0.55	0.62	0.83		0.63	0.72		0.68	0.43	0.63	0.35	0.46	0.76	0.47	0.43		0.48	0.61		
Sum	98.47	99.99	98.93		98.68	98.15		98.66	97.62		100.03	97.91		98.59	97.15		97.90	97.72		98.35	98.38		98.29
V	1.85			0.51			0.29			0.35			1.15			0.66			1.02			0.96	1.51
Cr	0.076			0.008			0.005			0.003			0.008			0.010			0.002			0.007	0.113
Zn	0.17			0.18			0.10			0.13			0.15			0.16			0.14			0.13	0.18
Uvsp (mol%)	0.248	0.347	0.628		0.747	0.830		0.568	0.610		0.608	0.441		0.407	0.557		0.384	0.453		0.415	0.520		0.387
Mgt (mol%)	0.752	0.653	0.372		0.253	0.170		0.432	0.390		0.392	0.559		0.593	0.443		0.616	0.547		0.585	0.480		0.613
For QUILF calculation																							
N Ti	0.249	0.334	0.581		0.697	0.779		0.534	0.565		0.567	0.422		0.388	0.524		0.361	0.425		0.395	0.479		0.389
N Mg		0.014	0.032		0.033	0.045		0.034	0.039		0.036	0.024		0.019	0.025		0.026	0.024		0.027	0.033		
N Mn	0.003	0.008	0.015		0.017	0.015		0.010	0.012		0.014	0.009		0.015	0.015		0.011	0.013		0.012	0.010		0.006

Microprobe analyses with a defocussed beam.
All analyses recalculated following Lindsley's method (QUILF algorithm; Andersen et al., 1993).

sandwich intergrowths are particularly well developed in the upper and lower part of the intrusion, where the opaque mineral content is lower and where the magnetite is subordinate to ilmenite.

Ilmenite grains are homogeneous in FLI, the hematite content being below the threshold of hematite exsolution (Table 2). Grain boundaries with cloth-textured magnetite are generally sharp, often straight and exempt of reaction rims (Fig. 4B). This is rather surprising because evidence of subsolidus reaction between the two oxides is rather common in plutonic rocks. Clear examples have been documented in the Bjerkreim-Sokndal layered intrusion (Duchesne, 1970, 1972), where compositional readjustment took place to relatively low temperatures and produced a variety of contact textures (spinelliferous ilmenite rims, zoning of hematite exsolution in ilmenite).

The composition of cloth-textured magnetites is easily determined by electron microprobe using a defocused beam. The bulk composition of trellis-textured grains cannot, however, be determined in this way, the only possible approach being to separate the magnetite and measure its bulk composition by XRF. This method was used in samples 13 and 289, in which cloth-textured grains are absent (Table 1). Interestingly, microprobe analyses of cloth-textured magnetites may show different compositions from grain to grain, and with XRF bulk analyses on separated fractions (Fig. 6 below). In some samples the variation from grain to grain is minor and close to the bulk composition (e.g. 204, 113 and 69); in others the composition interval can be large and the bulk (average) composition lower (e.g. 137.5) than the minimum value. Two processes can, together or separately, account for this variation. First, reaction between magnetite and ilmenite grains which are in contact (interoxide reaction of Frost et al., 1988) can lower the Ti content of the magnetite grain. The amplitude of the decrease depends on the size of the contact zone between the two oxides, and thus can vary from grain to grain (see e.g. Duchesne, 1972). Second, oxidation of magnetite to form a trellis microtexture can develop external granules which might be removed during the separation process. In sample 137.5, the bulk composition (Table 1) is low in TiO_2, but particularly high in V compared to neighbouring samples (Fig. 6), and shows an anomalously high distribution coefficient between magnetite and ilmenite. This anomaly can readily be explained by concentration of V in magnetite that has lost part of its V-poor ilmenite content as a result of external granule exsolution. It is worth noting that this variation in TiO_2-content affects the various samples to different extent, probably due to slightly different subsolidus T–fO_2 evolution. In magnetite 228, the higher TiO_2-content of the separated fraction relative to the microprobe analyses may reflect contamination by primary ilmenite during mineral separation.

Table 2
Chemical compositions (XRF analyses) of separated ilmenite fractions from the Fedorivka layered intrusion

Sample	13	37	69	113	137.5	180	204	228	289
SiO_2	0.57	0.38	0.49	0.64	0.22	0.23	0.76	0.71	0.58
TiO_2	49.37	51.06	52.05	51.50	51.59	51.29	50.47	51.21	49.38
Al_2O_3	0.00	0.11	0.00	0.00	0.07	0.07	0.00	0.00	0.00
Fe_2O_3	5.56	2.79	0.97	1.81	1.99	2.53	3.55	2.20	5.65
FeO	42.36	44.01	44.56	43.89	44.17	43.93	42.98	43.59	42.09
MnO	1.21	0.91	1.30	1.49	1.30	1.28	1.48	1.54	1.45
MgO	0.43	0.53	0.49	0.48	0.48	0.48	0.46	0.47	0.41
CaO	0.15	0.14	0.13	0.15	0.10	0.09	0.16	0.16	0.12
V_2O_3	0.35	0.07	0.02	0.04	0.07	0.10	0.15	0.12	0.33
Trace elements (ppm)									
Zn	108	80	29	59	50	62	62	54	110
Nb	93	59	35	56	54	52	57	47	55
Zr	414	162	74	188	164	125	114	127	120
Hem (mol%)	0.056	0.028	0.010	0.018	0.020	0.025	0.036	0.022	0.057
Ilm (mol%)	0.944	0.972	0.990	0.982	0.980	0.975	0.964	0.978	0.943
For QUILF calculations									
Xgeik	0.017	0.020	0.019	0.019	0.019	0.019	0.018	0.018	0.016
Xpyr	0.027	0.020	0.029	0.033	0.028	0.028	0.033	0.034	0.033
Xhem	0.053	0.027	0.009	0.017	0.019	0.024	0.034	0.021	0.054
Xilm	0.903	0.933	0.943	0.931	0.934	0.929	0.915	0.927	0.897

All analyses recalculated to 100 and FeO calculated following Lindsley's method (QUILF algorithm, Andersen et al., 1993).

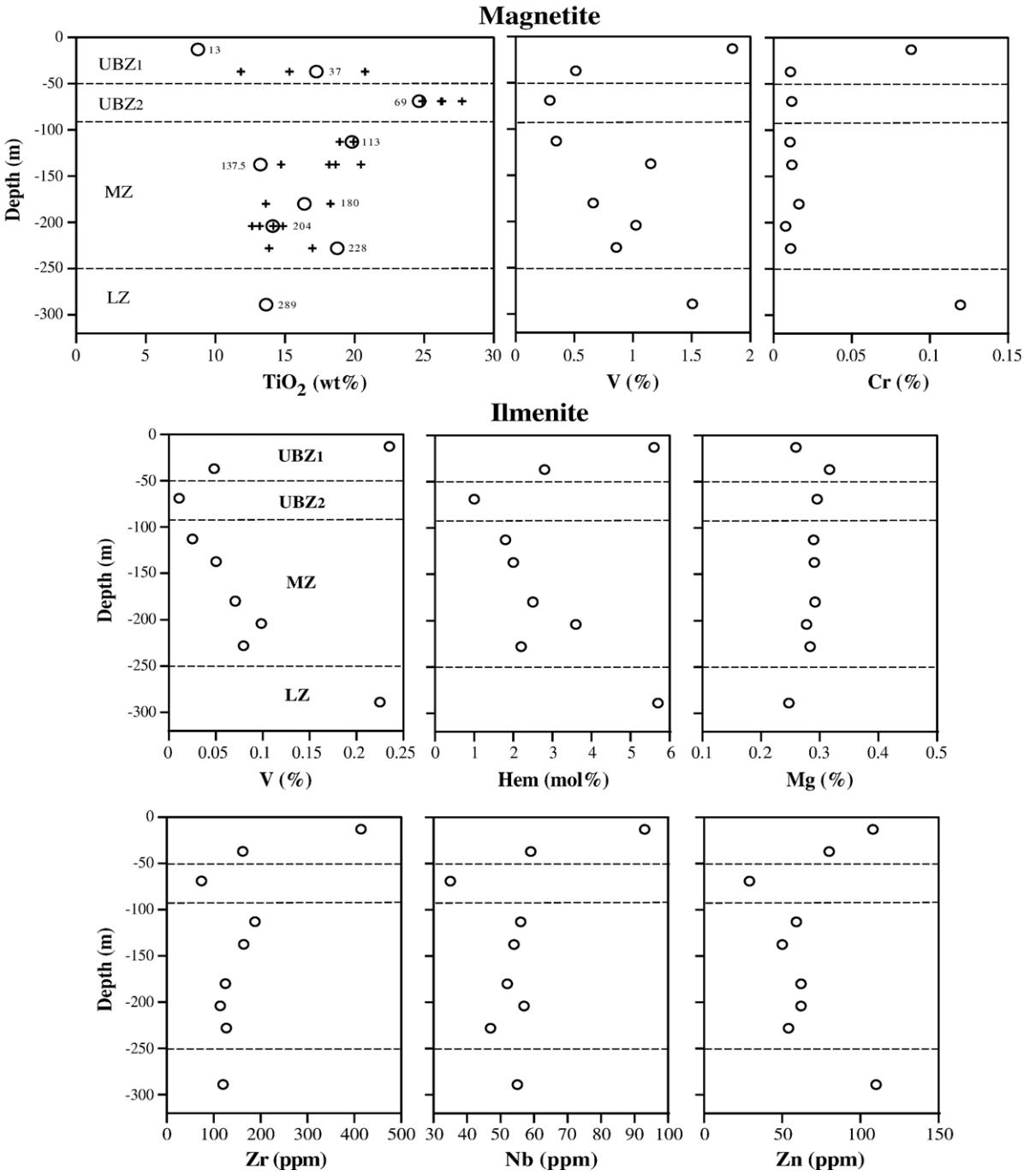

Fig. 6. Stratigraphic variations in magnetite and ilmenite compositions across the whole intrusion. +=electron microprobe analysis with a defocused beam; ○=XRF determination on separated magnetite fractions.

3.3. Subdivisions of the layered series

On the basis of detailed petrographical investigation of the core material from drill hole 581, which penetrates on the maximal thickness of the intrusion, we are able to distinguish four major stratigraphic units, which essentially differ from each other by the relative abundance of the main minerals and their cumulus or intercumulus nature (Fig. 5). Plagioclase, olivine, augite and ilmenite are present throughout the intrusion and are considered as constant cumulus phases. The status of apatite and magnetite varies from zone to zone.

Lower Zone (LZ) 322.2 m (bottom contact) −250 m. The lowermost unit consists of mesocratic olivine gabbro, characterized by the relatively uniform abundance of the main rock-forming minerals (no banding). The main feature of this unit is the relatively low abundance of apatite (0 to 4 vol.%) and the high ratio ilmenite/magnetite (magnetite is a rare mineral). Some samples are totally devoid of magnetite. Magnetite and apatite are interpreted as intercumulus minerals. A few large inclusions (xenoliths) of enclosing anorthosite are present.

Middle Zone (MZ) 250–90 m. This is the thickest zone and consists of meso- to melanocratic gabbro. Modal layering is well developed in the lower part, becoming sporadic upwards. Apatite is a cumulus phase. Ti-rich magnetite is also an abundant cumulus mineral but still occurs in lesser amounts than ilmenite.

An Upper Border Zone, which can be divided into two subzones:

Upper Border Zone 2 (UBZ_2) 90–50 m. The low plagioclase content gives this subzone a distinct melanocratic character. Magnetite is the dominant Fe–Ti oxide mineral (magnetite/ilmenite ratios 10:4); it is Ti-rich. Apatite is a cumulus phase.

Upper Border Zone 1 (UBZ_1) 50 m-surface (under sedimentary cover). This subzone is relatively plagioclase-rich (average 41 vol.%); the dominant lithology is mesocratic olivine gabbro. Magnetite is a minor phase. In the relatively leucocratic character and the low abundance of magnetite this subzone resembles the LZ, but the presence of prismatic apatite in relatively large amounts is a distinctive feature of UBZ_1.

This subdivision has been extended to a complete section through the intrusion (A–B in Fig. 2A) by inspection of five other boreholes. Our interpretation of the internal structure is shown in Fig. 2B. The internal structure appears to be asymmetrical: LZ wedges out laterally to both sides; MZ wedges out to the east and reaches the surface in the northwestern part of the intrusion; UBZ_2 has a similar shape to MZ, and UBZ_1 is restricted to the uppermost portion to the SE.

4. Variation of mineral composition with stratigraphy

Major and minor element compositions of minerals at various levels in borehole 581 were determined by electron microprobe and by XRF on separated minerals (see Appendix A). The data are reported in Tables 1 and 2 and B1–B4 (on-line supplement), and the compositional variations in stratigraphic height are plotted in Figs. 5–7.

The Fo-contents of olivine and the mg# of augite show essentially parallel trends in Fig. 5. Starting

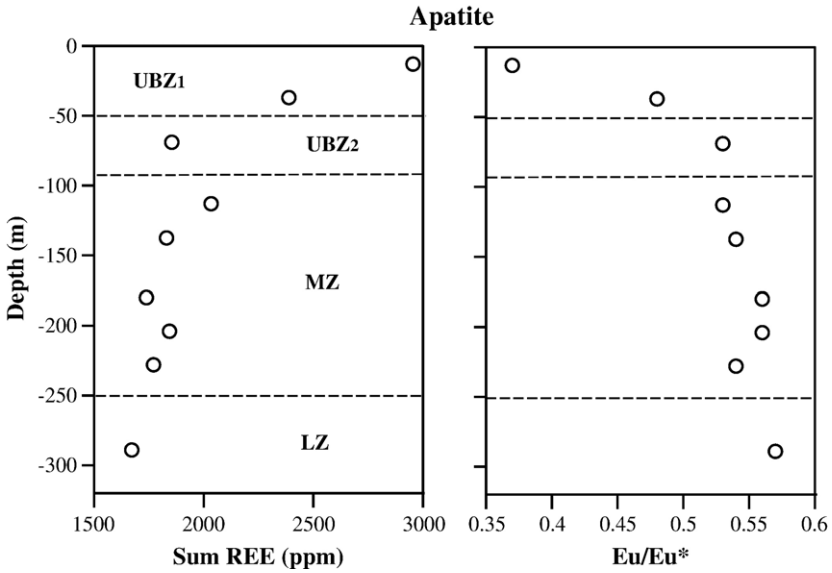

Fig. 7. Stratigraphic variations in apatite compositions in drill core 581. Eu/Eu∗ is the Eu anomaly (see Table B4 on-line supplement for analytical data).

from relatively magnesian compositions in LZ (Fo_{46} and cpx mg# 0.64), they become steadily more evolved up through MZ, then abruptly more so in UBZ_2 (Fo_{32} and cpx mg# 0.50), followed by a reversal up to more magnesian compositions in UBZ_1. The An-content of plagioclase (Fig. 5) is fairly constant (ca. An_{43}) in LZ and the base of MZ, then decreases to An_{39} at the top of MZ, above which it rapidly increases to An_{45} at the UBZ_1. The Sr-content of plagioclase (Table B2 on-line supplement) shows an increase from ca. 770 ppm in LZ to a maximum of 870 ppm at the top of MZ, then decreases to lower values (ca. 800 ppm in UBZ).

TiO_2 in magnetite shows no clear variation in LZ and the lower part of MZ, but increases steadily from the uppermost part of LZ up to UBZ_2, then sharply decreases in UBZ_1 (Fig. 6). V in magnetite is inversely correlated with TiO_2. It decreases erratically up to UBZ_2, then increases up to 1.85% V in the topmost sample (Fig. 6). Cr remains close to the detection limit except at the base and top of the section, where it reaches values ca. 0.1% (Fig. 6). Zn varies between 0.12% and 0.16% with a minimum at 0.09% in UBZ_2. The evolution in ilmenite (Fig. 6) is essentially parallel to that in magnetite for V and hematite content (Hem). Mg in ilmenite increases slightly from LZ to MZ where it remains quite constant before decreasing in UBZ_1. Zr and Nb do not vary much up to UBZ_2 where they abruptly decrease, followed by a sharp increase upwards. A similar trend is also shown by Zn in the upper part of the section.

REE in apatite (Fig. 7) increase somewhat from LZ to the top of MZ, then decrease in UBZ_2 before they increase rapidly in UBZ_1. The Eu-anomaly decreases markedly in UBZ_1.

In brief, the compositional variations in MZ are generally smooth and continuous for all minerals and elements. UBZ shows an inverse relation, which in some case is shifted to lower values. Mineral compositions in LZ are less evolved than in the MZ. UBZ_1 minerals show at the same time less evolved characters as in LZ, and conspicuous enrichments in incompatible (magmaphile) elements, such as REE, Zr and Nb.

5. Whole-rock compositional evolution

The whole-rock compositions of 34 samples from borehole 581 and 4 samples from the upper part of borehole 599 are reported in Tables 3 and B5 (on-line supplement), and major element compositions are plotted in Harker diagrams (Fig. 8). The analysed samples were selected to represent all petrographic types, including mafic and felsic layers.

Table 3
Major and trace element whole-rock compositions of selected samples from the Fedorivka layered intrusion (boreholes 581; sample number is equivalent to depth in meters)

Sample	Borehole 581					
Zone	13	69	113	204	228	285
	UBZ_1	UBZ_2	MZ	MZ	MZ	LZ
Major elements (wt.%)						
SiO_2	35.48	32.83	32.11	31.75	32.52	38.71
TiO_2	5.87	5.22	6.38	7.2	6.7	6.65
Al_2O_3	9.78	6.47	5.94	6.12	7.53	9.12
Fe_2O_3	25.88	33.74	30.36	30.97	28.94	23.04
FeO	21.15	26.80	23.97	23.85	22.32	
MnO	0.29	0.39	0.33	0.32	0.3	0.27
MgO	6.73	6.87	7.83	8.55	7.78	7.73
CaO	9.75	9.92	11.41	10.23	10.48	10.14
Na_2O	1.82	1.1	1.03	1.13	1.42	2.90
K_2O	0.43	0.23	0.22	0.18	0.23	0.33
P_2O_5	3.38	2.74	3.7	3.15	3.34	1.47
Total	99.41	99.51	99.31	99.60	99.24	100.36
MgO/FeOt	0.29	0.23	0.29	0.31	0.30	0.37
Trace elements (ppm)						
U	0.23	0.11	0.16	0.1	0.1	0.05
Th	1.27	0.35	0.39	0.33	0.33	0.5
Zr	74	28	41	33	28	36
Hf	2.4	0.74	1.2	1.01	1.04	1.34
Nb	16	4	7	7	5	9
Ta	0.67	0.16	0.44	0.52	0.45	0.69
Rb	10.0	4.4	4.7	6.4	4.4	5.0
Sr	356	248	256	262	296	294
Ba	349	162	198	180	213	296
Ni	23	20	14	26	25	33
V	364	322	240	822	813	356
Zn	171	169	170	178	166	125
Co	53	45	55	63	60	63
Cu	92	77	99	108	100	84
Ga	9.4	10.7	11.3	8.5	9.6	11.6
Pb	3	2	5	2	3	5
Y	55	36	51	42	43	23
La	33	19	30	21	23	11
Ce	89	55	85	66	72	31
Pr	14.5	8.4	13.02	9.96	10.7	4.78
Nd	63.7	39.7	59.5	44.1	49	24.4
Sm	14.3	9.8	14.2	11.9	13.2	6.2
Eu	2.7	2.0	2.9	2.1	2.6	1.7
Gd	11.9	8.0	12.1	9.1	9.7	5.4
Tb	1.7	1.1	1.7	1.2	1.3	0.7
Dy	8.1	5.6	8.7	6.5	7.1	4.1
Ho	1.7	1	1.56	1.22	1.26	0.76
Er	3.3	2.17	3.65	2.77	3.02	1.95
Tm	0.52	0.28	0.46	0.36	0.37	0.27
Yb	2.6	1.4	2.6	1.9	2.1	1.5
Lu	0.35	0.22	0.35	0.26	0.27	0.22
Sum REE	248	154	235	177	196	94

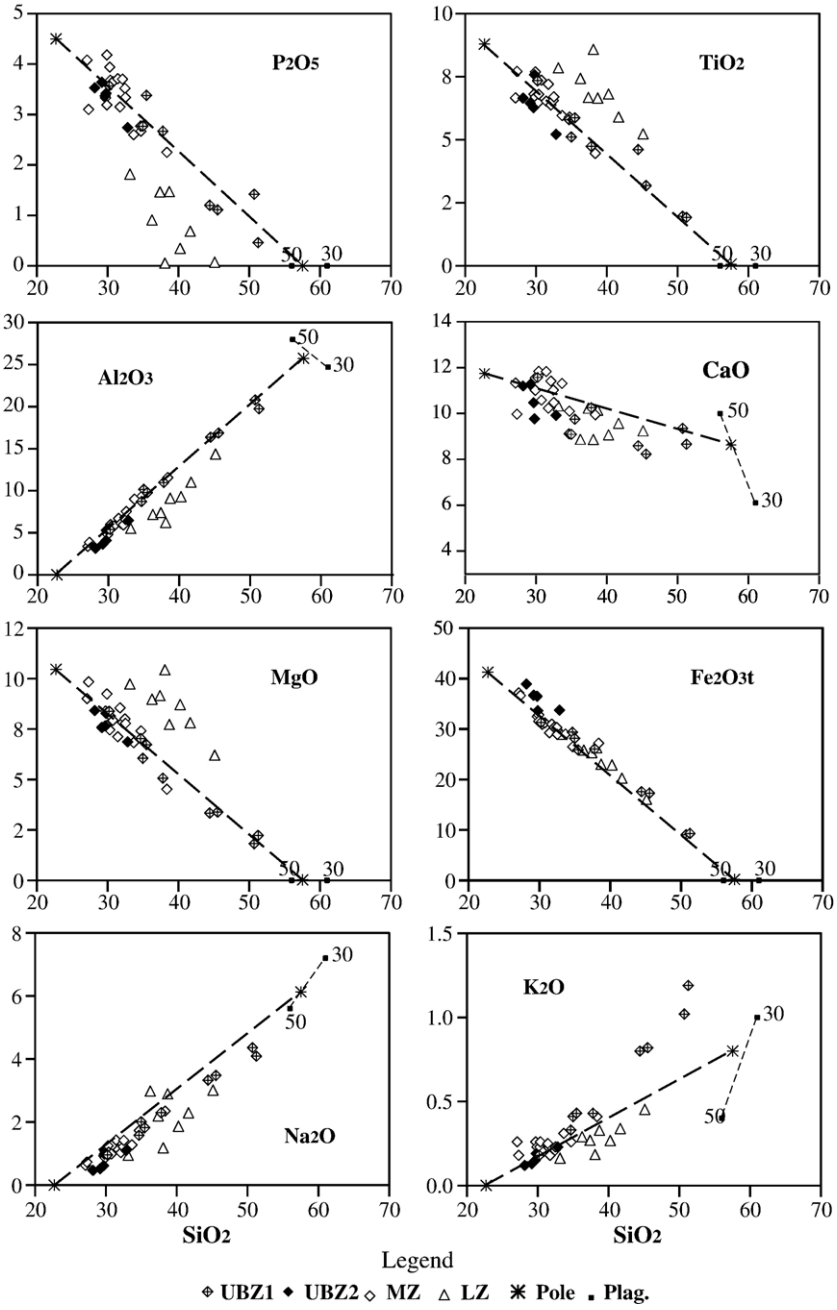

Fig. 8. Harker diagrams of Fedorivka whole-rock compositions (Table 3 and on-line supplement Table B5 for analytical data). The various symbols refer to the 4 stratigraphic units. The compositions of the plagioclase and mafic poles, valid for MZ, are shown together with plagioclases with compositions An_{50} and An_{30}, joined by a dashed line. The correlation coefficients *r* of group of samples including MZ cumulates and plagioclase pole vary between 0.930 (P_2O_5) and 0.996 (Al_2O_3), except for CaO (0.526). The dispersion of the CaO values is due to the fact that the mafic pole value for CaO accumulates small fluctuations in the modal proportions of three minerals, viz. plagioclase, Ca-rich pyroxene and apatite (see Duchesne and Charlier, 2005, for a thorough discussion of the 2-pole concept). All concentrations in wt.%.

5.1. Major element evolution

It emerges from Fig. 8 that the LZ samples are quite distinct from the others, particularly in P_2O_5 and MgO contents, in agreement with the lower apatite content and the less evolved character of the mafic minerals. The bulk MgO/FeOt ratio varies from 0.40 ±0.03 in LZ to 0.27±0.03 in the other zones.

Table 4
Chemical compositions of the mafic and plagioclase poles, and normative composition (wt.%) of the mafic pole and cotectic assemblage

	Mafic pole	Plagioclase pole
SiO_2	22.72	57.54
TiO_2	8.79	
Al_2O_3	0.00	25.74
Fe_2O_{3t}	41.27	
Fe_2O_3	5.26	
FeO	32.47	0.18
MnO	0.45	
MgO	10.46	
CaO	11.74	8.63
Na_2O	0.00	6.13
K_2O	0.00	0.80
P_2O_5	4.50	
Total	99.93	99.02
		An=41.7%

Normative composition (wt.%)

	Mafic pole[a]	Cotectic assemblage
Plagioclase		49.4
Olivine	40.5	20.5
Augite	20.8	10.5
Ilmenite	11.2	5.7
Magnetite	15.0	7.6
Apatite	12.0	6.1
Total	99.5	99.7

[a] Calculated by least-square regression with average mineral compositions.

Except for slightly higher Fe_2O_{3t} contents in UBZ_2, samples from MZ and UBZ_2 are rather similar in Fig. 8; the most mafic UBZ_1 samples also overlap with the MZ trends. In keeping with the leucocratic character of the rocks in this sub-zone, the UBZ_1 samples are enriched in plagioclase component.

Interestingly, all the samples from MZ tend to define linear trends, extending from a plagioclase pole to a mafic pole (Fig. 8). The plagioclase pole can be defined as the average composition of MZ plagioclases (An_{42}) and the mafic pole can be calculated graphically or algebraically, assuming it is devoid of plagioclase and does not contain Al_2O_3, Na_2O and K_2O (Table 4). The rocks which plot on these trends have the same mineral association, i.e. plagioclase, olivine, augite, apatite, ilmenite and magnetite, and thus essentially differ from each others in the modal proportion of plagioclase compared to all other minerals. Moreover, the mafic minerals keep approximately the same proportions relative to their bulk mineral composition. Note that this mafic pole composition gives the maximum possible enrichment in TiO_2 and P_2O_5 to be found in the whole intrusion (i.e. 8.8% TiO_2 and 4.5% P_2O_5). This inference might be useful in the economic evaluation of the intrusion.

5.2. Trace element evolution

A principal component analysis of the major and trace element analyses is provided in Supplementary Fig. 1 and Table B6 of the on-line supplement. In view of this discussion, it is possible to investigate the trace element behaviour by looking at the evolution of selected trace elements throughout the layered sequence (Fig. 9). Again the LZ differs from the other zones by a significantly lower content of Y (low apatite content) and Zn (low magnetite content), and with some high Ni values, possibly due to traces of sulphides. The appearance of magnetite as a cumulus mineral at the base of the MZ is clearly marked by high V and Zn contents. The decrease of V through the MZ (although there is no substantial change in mineral proportions

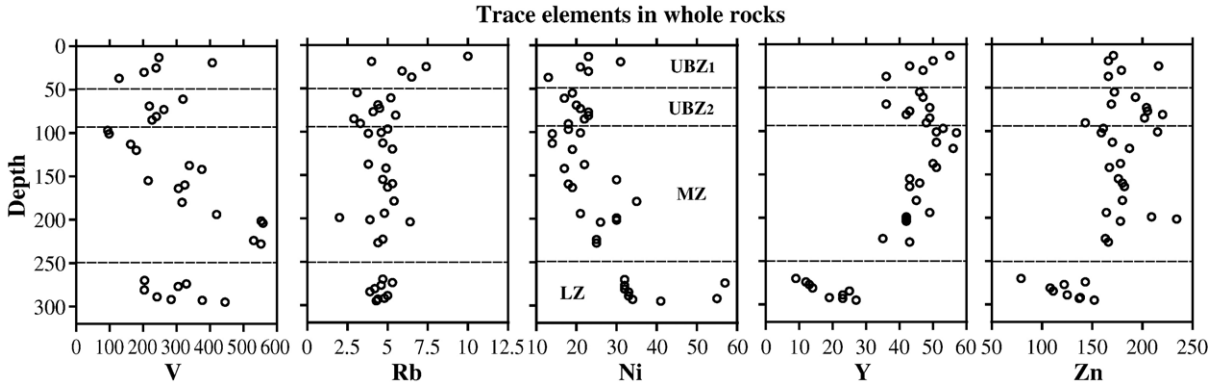

Fig. 9. Stratigraphic variation of selected trace element concentrations in whole-rock samples along drill core 581 (see Table 3 and on-line supplement Table B5 for analytical data).

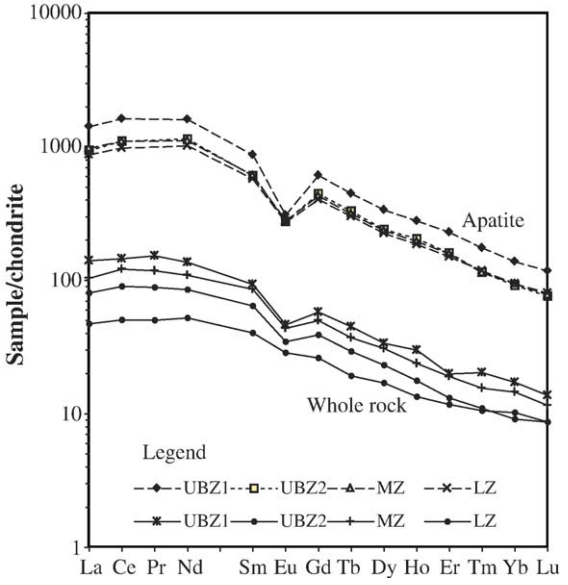

Fig. 10. Chondrite-normalized REE distribution in whole-rock samples and apatite separates from the various zones of the Fedorivka intrusion. Samples from the same zone have been averaged. Normalizing values from Sun and McDonough (1989). Note the similarities between apatite and whole rocks which result from the REE controlling effect of apatite (see on-line supplement Table B4 for analytical data).

through MZ) is good evidence that this element is decreasing in the conjugated melts in the magma chamber. Similarly the abrupt increase in Y from the LZ to the MZ is a consequence of the appearance of apatite as a cumulus mineral. Rb (strongly correlated to Nb and Zr) increases upwards in UBZ_1. In LZ the continuous upwards decreases of Y, V, and Zn reflect a decrease in magnetite and apatite contents upwards, both minerals being intercumulus. Note, however, that Rb remains fairly low (close to detection limit) and constant in LZ. Finally the REE are strongly correlated with the P-content and controlled by the apatite distribution (Fig. 10).

6. Discussion

6.1. Evidence of fractional crystallization

The LZ is the least evolved lithological unit of the FLI. It contains the most magnesian olivines and augites (Fig. 5); ilmenite, a major rock-forming mineral, is rich in V, Cr, and Hem (Fig. 6); Ni in whole-rock composition reaches maximum values in some LZ samples (Fig. 9). As already noted in the petrographic description, some LZ samples are devoid of apatite and magnetite. This strongly suggests that these minerals are not cumulus phases and do not belong to the primary mineral assemblage of the LZ. Actually, apatite and magnetite must have crystallized from the trapped liquid fraction. In theory, their trace element compositions reflect the composition of the melt with which they last equilibrated, not that of the magma from which the cumulus minerals formed. In the present case, however, the difference is bound to be small for elements strongly compatible with magnetite and apatite, because the trapped liquid was close to saturation in these minerals which become liquidus phases soon after, in the MZ. We can thus accept, as a first approximation, that the high contents of V and Cr in intercumulus magnetite from the LZ reflect the high contents of these elements in the conjugated magma. For similar reasons, the REE-content of LZ apatite is a good proxy for the REE-contents of the magma.

The MZ is more evolved than LZ and shows clear evidence of fractional crystallization upwards. The Fo in olivine, the mg# in augite, and An in plagioclase steadily decrease throughout, An reaching a minimum value at the top of MZ (Fig. 5). V in ilmenite and magnetite decreases by a factor 3 in the separated samples (Fig. 6), and this behaviour of V is reflected in the whole-rock composition (Fig. 9), where the decrease is by a factor 6 in the entire range of samples from bottom to top of MZ. REE in apatite slowly increase (Fig. 7), thus showing that, despite the occurrence of the apatite in the liquidus assemblage, the residual liquid gradually became enriched in REE. This increase implies bulk partition coefficient below unity, which in turn implies rather low partition coefficients for REE between apatite and the melt, as noted by Charlier et al. (2005) in the Bjerkreim-Sokndal layered intrusion. All compositional variations of the minerals are rather smooth and in continuity with the LZ. There is no indication of any replenishment by a more primitive magma during the differentiation in LZ and MZ.

We therefore conclude that the 140-m-thick MZ formed by fractional crystallization of a single batch of magma remaining after crystallization of the LZ.

6.2. Compositional reversal through the UBZ

In contrast to the LZ and MZ, the UBZ is characterized by a reverse evolution. This is manifested by the olivine Fo-content, augite mg# and plagioclase An (Fig. 5), as well as V and Hem in ilmenite and V and Cr in magnetite (Fig. 6). The immediate conclusion is that the UBZ results from a crystallization process starting at the roof of the intrusion and progressing downward. Compositional reversal of this type was first described from the Skaergaard intrusion (see the review

in McBirney, 1996), so we have used the same zone name and reverse numbering by analogy to this classical case.

The UBZ evolution, however, does not exactly mirror the evolution in LZ and MZ. First, some trends, such as the Fo and augite mg#, are shifted to lower values in UBZ. Second, some elements are enriched towards the top of UBZ, such as Zr, Nb, and Zn in ilmenite (Fig. 6), REE content and size of the Eu anomaly in apatite (Fig. 7), Rb, Nb, and Zr in whole-rock compositions (Fig. 9), contrasting with their lower abundances in LZ and base of MZ. The UBZ displays hybrid characteristics between primitive features, shown by compatible elements, and highly evolved ones, shown by incompatible elements. We interpret this hybrid nature as resulting from a mixing process between cumulus minerals and intercumulus trapped liquid, the latter being enriched in incompatible elements and having a high Fe/Mg ratio. The compositional shift of olivine, and to a lesser extent of augite, due to reequilibration with trapped liquid, is larger than that of plagioclase (Fig. 11). This results from the slow NaSi–CaAl exchange in plagioclase (Grove et al., 1981), which is known to retain its primary composition, as well as to the larger amount of plagioclase compared to pyroxene and olivine (Barnes, 1986). The difference in the compositional shifts also probably results from a larger contrast between the mg# of the liquid compared to those of olivine and augite, higher than the difference in the anorthite content between the trapped liquid and plagioclase. Similar shifts in mafic composition relative to the plagioclase composition have been described in other layered intrusions, such as the Stillwater Complex (McCallum, 1996) and the Skaergaard intrusion (McBirney, 1996). Moreover, crystallization of the interstitial liquid, enriched in incompatible elements, has increased the content of these elements in the bulk rock (e.g. Rb, K) and also in the minerals in which they are compatible (e.g. Zr and Nb in ilmenite).

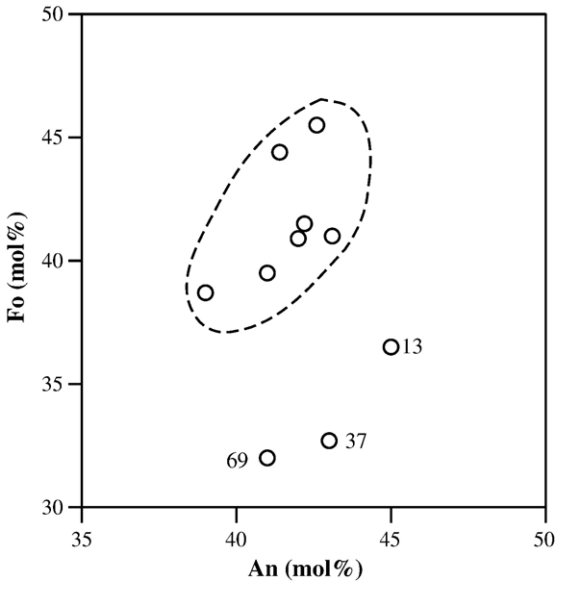

Fig. 11. Olivine Fo-content vs. plagioclase An-content in cumulate from the Fedorivka layered intrusion. Samples 13, 37 and 69 from the UBZ are clearly lower in Fo content due to re-equilibration with a higher proportion of trapped liquid.

The reverse evolution in UBZ is actually the result of two processes. The first is the crystallization from the roof of progressively more evolved cumulus assemblages, which mirrors the LZ; the second is a downward decrease in the trapped liquid fraction, which explains the downward decrease in incompatible element concentrations (see the Y and Rb evolution in Fig. 9). The closer to the roof of the intrusion, the greater the cooling rate of the crystallizing mush, so that extraction of the trapped liquid becomes more difficult by filtering through the cumulus mineral framework. The behaviour of incompatible elements in the UBZ can be accounted for by this simple mechanism.

As previously mentioned for the LZ, the continuous upwards decreases of Y, V, and Zn in whole-rocks, incorporated in intercumulus apatite and magnetite, also reflect a decrease in the trapped liquid fraction from the lower contact with the host anorthosite to the center of the intrusion. Similar scenarios have been invoked for the Teksevatnet cumulates in the Bjerkreim-Sokndal intrusion (Charlier et al., 2005), as well in a number of layered intrusions (e.g. Hoover, 1989).

6.3. The trapped liquid fractions in UBZ_1 and LZ

Mineral associations and compositional trends in the UBZ_1 and LZ are similar, but not identical. Apatite and magnetite are interpreted as intercumulus phases in both zones, with a higher proportion of these phases in the UBZ_1. This discrepancy results from the crystallization of a higher proportion of trapped liquid at the top of the intrusion.

The lower trapped liquid fraction at the bottom of the intrusion can be explained by extraction of part of the intercumulus melt by compaction of the crystal mush under the lithostatic pressure of the high density cumulate pile. Moreover, we will show below that the interstitial liquid was close to a monzonitic composition. Therefore, a buoyant behaviour, driven by the density difference with the cumulus assemblage, could also

have favoured the segregation process. These two processes can account for the higher trapped liquid fraction in the upper part compared to the bottom of the intrusion.

In our petrographic study of the UBZ and LZ samples, no interstitial quartz or granophyric products have ever been observed that would unequivocally represent the crystalline products evolved trapped liquid. The only indication that some rocks are actually cumulates with a high trapped liquid fraction (orthocumulates) is their geochemical features, as discussed above. The absence of evolved material and quartz among intercumulus phases can be explained by equilibrium, rather than by fractional crystallization of the trapped liquid.

On the scale of the whole intrusion, the absence of granophyric rocks or equivalent felsic material representing the residual liquid of the fractionation process is conspicuous. It may be that this liquid, possibly laden with minerals, escaped to a part of the intrusion that has subsequently been eroded away. The asymmetry of the trough structure (Fig. 2) might have permitted these residual melts to filter off the MZ cumulates along the northwestern contact of the intrusion. The magma chamber was thus open during differentiation.

6.4. Composition of the melt in equilibrium with MZ cumulates

The composition of melts in equilibrium with evolved cumulates in ferrobasaltic systems is highly debated. In the Skaergaard intrusion, some authors, following Wager and Brown (1968), consider that the melt that gave rise to the evolved cumulates was Fe-enriched, even after the crystallization of magnetite (e.g. McBirney, 1975; McBirney and Naslund, 1990). This conclusion was questioned by Hunter and Sparks (1987) who suggested that these liquids became silica-enriched after magnetite appeared on the liquidus. Later, the iron-enrichment model found some support in the evolution of the Fe-content in plagioclase (Tegner, 1997) and of the V-content in pyroxene (Jang et al., 2001). On the other hand, silica-enrichment was obtained in the experimental melts of Toplis and Carroll (1994).

In the Rogaland anorthosite province, the study of jotunites, formerly called monzonorites (Michot and Michot, 1969; Duchesne et al., 1985, 1989; Duchesne, 1990), has shed new light on this question. Jotunite occurs as dykes or chilled margins to andesite anorthosite bodies, such as the Bjerkreim-Sokndal layered intrusion (Duchesne and Hertogen, 1988; Wilson et al., 1996) and the Hidra body (Demaiffe and Hertogen, 1981). The dykes themselves display a series of chills extending continuously from ca. 47% SiO_2 (hypersthene monzodiorite or jotunite) to >66% SiO_2 (granite or charnockite). On the other hand, the Bjerkreim-Sokndal layered intrusion displays a thick and varied series of cumulates resulting from fractional crystallization of a jotunitic melt. This cumulate series has been shown to be conjugated to the dyke melt series (Vander Auwera et al., 1998b). In a first attempt to model the continuous melt evolution in the Tellnes dyke from jotunite to charnockite, Wilmart et al. (1989) calculated the composition of olivine in equilibrium with the melts using the algorithms of Ford et al. (1983). These values permitted to define the crystallizing assemblages in the Bjerkreim-Sokndal series of cumulates. Mass balance calculations were then used to determine the mineral proportions in the crystallizing assemblages. It emerged from this that a cumulate (C3) made up of plagioclase (An_{37})+olivine (Fo_{50})+Ca-rich pyroxene (mg# 67)+ilmenite (Hem_4)+magnetite (Usp_{35})+apatite, similar to cumulates at the base of the Transition Zone in the upper part of the layered series of Bjerkreim-Sokndal, was in equilibrium with a melt with the composition of sample 78-28 (57% SiO_2), and subtraction of C3 from this melt would drive it towards granitic (charnockitic) compositions (>66% SiO_2) (Fig. 12; Table 5). Later, experimental results (Vander Auwera et al., 1998b) led to a refinement of the model and of the C3 assemblage (at the pressure conditions of crystallization of the dyke, the olivine actually reacted to pigeonite and quartz). These approaches showed unambiguously that a silica-rich melt was in equilibrium with evolved cumulates, thus supporting the views of Hunter and Sparks (1987) and Toplis and Carroll (1994) for the Skaergaard evolution.

Recent experimental data (Toplis and Carroll, 1994) allow refinement of the composition of olivine in equilibrium with an evolved melt. The Mg/Fe olivine/melt partition coefficient of 0.32 ± 0.2, according to Roeder and Emslie (1970), has been shown by these authors to be only valid for mg#>0.30 in the melt, and to vary linearly up to 0.40 with the decrease of mg# to 0.15. In the case of melt 78-28, the ferrous–ferric iron ratio at various fO_2 being estimated following Kilinc et al. (1983), calculation of the olivine composition gives $Fo_{45 \pm 2}$ at FMQ and $Fo_{42 \pm 2}$ at two log units below FMQ. Since these values are very close to the olivine composition in Fedorivka MZ cumulates ($Fo_{38–42}$), we can conclude that the latter were in equilibrium with a melt of monzonitic composition with a mg# similar to 78-28.

In a previous section and in Fig. 8, it has been shown that the MZ cumulate composition can be approximated

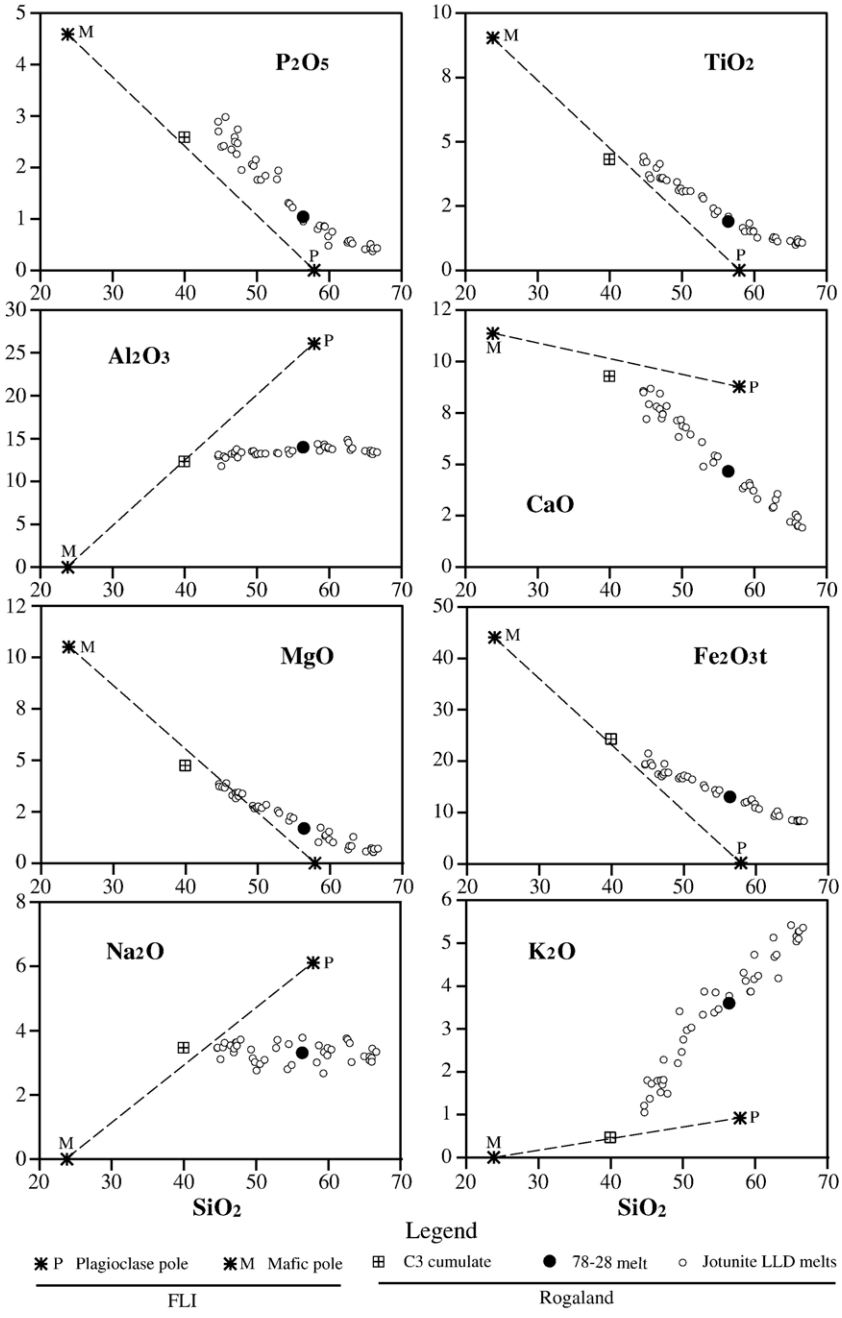

Fig. 12. Harker diagrams showing the relationships between the Rogaland jotunitic LLD (liquid line of descent; Vander Auwera et al., 1998b), in which sample 78-28 has been shown to be in equilibrium with C3 cumulate, and the 2-pole linear trend characteristic of MZ cumulates (see text). All concentrations in wt.%.

by a mixture of a mafic pole of fixed composition and a plagioclase pole (Table 4). This feature of the Fedorivka MZ cumulates can be compared with the Bjerkreim-Sokndal layered intrusion, where the 2-pole cumulate concept was developed (Duchesne and Charlier, 2005), with a variety of implications for the formation of cumulates (e.g. lack of gravity sorting, lack of immiscibility, in situ growth). The linear trends in the FLI MZ cumulates are, however, not so clearly defined as in Bjerkreim-Sokndal, thus some gravity sorting of the mafic minerals cannot be precluded. Nevertheless, the 2-pole cumulate concept provides a useful means to assess the cotectic composition of the MZ cumulates at this stage of the Fedorivka melt evolution. The linear trend is indeed a

Table 5
Major element compositions (wt.%) of C3 cumulate and conjugated melt 78-28 (after Vander Auwera et al., 1998b).

Sample	C3	78-28
SiO_2	39.93	57.02
TiO_2	4.32	1.92
Al_2O_3	12.33	13.31
FeOt	21.91	11.98
MgO	4.75	1.71
CaO	9.29	4.71
Na_2O	3.47	3.35
K_2O	0.47	3.64
P_2O_5	2.59	1.05
Total	99.06	98.69

geometrical locus of the cotectic composition (Duchesne and Charlier, 2005). It is striking that the C3 composition also plots on or very close to that line (Fig. 12), giving further support to the hypothesis that the MZ cumulates were effectively in equilibrium with monzonitic melts.

The MZ cotectic cumulate is notably more plagioclase-rich than the average MZ cumulate (compare Figs. 8 and 12) though normally cotectic cumulate should correspond to the average cumulate (see e.g. Duchesne and Charlier, 2005). The discrepancy observed here can be explained by a too small number of studied samples, therefore by a biased sampling, and/or some plagioclase might have been discharged laterally from the magma chamber, possibly dragged by the residual liquid. The large density difference between plagioclase and mafic minerals might have favoured the process.

6.5. Thermobarometry

Using magnetite and ilmenite pairs and following the calculations of Spencer and Lindsley (1966) gives equilibrium temperatures below 400° and fO_2 below −25 log units, which indicates important interoxide reaction during subsolidus re-equilibration. In the absence of relic grains of the solidus magnetite and ilmenite (see Duchesne, 1972; Wilmart et al., 1991), it is not possible to evaluate the liquidus fO_2 conditions and the subsolidus evolution.

The peculiarities of the Fedorivka Fe–Ti oxide association however allow us to approach this issue in a different way. It has been shown above that in some samples (e.g. 204: base of MZ; 113: top of MZ; 69: UBZ_2), magnetite does not contain ilmenite lamellae but cloth-textured ulvöspinel exsolution, that remain preserved from oxidation. This precludes "oxy-exsolution" processes due to intraoxide reaction (Duchesne, 1970; Frost et al., 1988). Moreover, in these samples there is very little variation in the TiO_2 content of individual magnetite grains and a good agreement between this composition and that of the bulk magnetite measured on separated fractions. This, together with the lack of evidence for reaction between magnetite and ilmenite (no spinelliferous ilmenite rim, no zoning in the cloth microtexture) suggests that the magnetite has not changed its composition during subsolidus evolution. Since magnetite is far more abundant than ilmenite in sample 69 (UBZ_2), it is essentially the ilmenite that has readjusted its composition in the interoxide reaction during cooling (Frost et al., 1988). In other words, subsolidus re-equilibration has effectively taken place, but ilmenite was the only oxide involved in the compositional evolution, and the T–fO_2 evolution followed the magnetite isocompositional curve.

In order to assess the fO_2 value in MZ and UBZ_2 an estimate of the temperature of crystallization of these rocks is needed. This can be done by analogy with the Skaergaard intrusion and with experimental data. In the Sandwich Horizon of the Skaergaard intrusion the temperature obtained with the QUIlF equilibrium (Frost et al., 1988) is between 980 °C and 1030 °C, and Morse et al. (1980) have calculated temperatures varying from 1067 °C to 1140 °C using the olivine+magnetite+pyroxene association. A more accurate temperature estimate for the FLI can be obtained from the experiments on ferrobasalts of Toplis and Carroll (1994). The An-content of plagioclase (Toplis et al., 1994b) indicates liquidus temperatures of 1045 °C (An_{42}) at the base of MZ, and of 1030 °C (An_{38}) at the top of MZ. Using the Fo-content of olivine in sample 69 we can deduce 1020 °C (Fo_{32}) for the equilibrium temperature of the mafic minerals in UBZ_2. These temperatures applied to the Fe–Ti oxide equilibrium of Spencer and Lindsley (1966) lead to fO_2 of −9.3 and −9.8 log units at the base and top of MZ, respectively, and −11.8 log units in UBZ_2. It can thus be concluded that the Fedorivka magma underwent strong relative reduction during differentiation from $\Delta FMQ = 0.7$ log units down to values of −1.4 log units.

Now that the T–fO_2 conditions have been determined, it is possible to use the pyroxene QUIlF equilibria (Frost and Lindsley, 1992; Lindsley and Frost, 1992) to test whether the olivines at the base and top of MZ and in UBZ_2 were in equilibrium with the magnetites, or whether they underwent compositional readjustment during cooling. The results of the calculation with the QUILF program (Andersen et al., 1993) show that the calculated olivine compositions are identical with that in UBZ_2 and indistinguishable within error from those observed in MZ. This agreement corroborates the hypothesis, put forward above, that the

subsolidus fO_2–T evolution in UBZ_2 followed the magnetite isocompositional curve.

6.6. V in magnetite: further evidence of low fO_2

The V-content in magnetite is 1.85% V in LZ and is never below 0.27% elsewhere (Table 1). These values are very high for such an evolved association. For example, in the Bjerkreim-Sokndal Transition Zone, magnetite is very V-depleted, varying from 0.14% to 0.02% V (Duchesne, 1972). In the same intrusion, the most primitive rock of the entire layered series, leucotroctolite at the base of macrocyclic unit IV, contains magnetite with 0.7% to 0.5% V (Duchesne, 1972; Jensen et al., 1993). In the Bushveld Complex, the maximum V-content in magnetite at the base of the magnetite layers is 1.3% V (Cawthorn and Molyneux, 1986), and in Skaergaard, Vincent and Phillips (1954) report up to 1.2% V magnetite from the Lower Zone.

As noted by several authors (see the review by Toplis and Corgne, 2002), the crystallization of magnetite is controlled by fO_2 which determines the ferric–ferrous iron ratio of the magma. Oxidizing conditions promote magnetite crystallization at higher temperatures than under reducing conditions (Toplis and Carroll, 1994). In the same way, fO_2 also determines the $V^{3+}/V^{4+}/V^{5+}$ ratios. The partition coefficient of V^{3+} between magnetite and melt is much higher for V^{3+} than for V^{4+} and V^{5+}. The net result is an increasing partition coefficient $D^{mag/liq}$ with reducing conditions. Accepting a partition coefficient of V between ilmenite and melt $D^{ilm/liq}=11.0$ from the experimental data of Zack and Brumm (1998) and an average value of $K^{mag/ilm}=9$ from the distribution in FLI ilmenite–magnetite pairs, we obtain a $D^{mag/liq}$ value of 99. This value is higher than the value (26) adopted for the Skaergaard modelling by Jang et al. (2001), and thus would point to lower fO_2 conditions than in Skaergaard.

Magnetite appears for evolved olivine compositions (Fo_{42}) in the FLI series of rocks. This late appearance also points to low fO_2 conditions. Toplis and Corgne (2002) have proposed a model in which the late crystallization of magnetite permits the V-content of the melt to increase, and, combined with the increase of the bulk $D^{mag/liq}$, yields magnetite with very high V-contents. This model does not account for the occurrence of ilmenite, and thus is not strictly applicable to the Fedorivka intrusion where ilmenite was already on the liquidus when the magma was emplaced into the chamber. However, inversion of the LZ magnetite composition, using the value of the $D^{mag/liq}$ of 99, gives a melt composition of 150 ppm V, somewhat lower than the ca. 300 ppm of a plausible parental magma (Toplis and Corgne, 2002). This shows, at least qualitatively, that some depletion of V in the parental melt, due to the crystallization of ilmenite, could have taken place before intrusion, but would have maintained a sufficiently high V-content in the magma to yield a V-rich liquidus magnetite. Early crystallization of ilmenite can also explain the low Cr-content in the first liquidus magnetite and the resulting high V/Cr ratios.

6.7. Nature and origin of the FLI parental magma

Evidence has been presented above that the melt in equilibrium with the MZ cumulates had a monzonitic composition. Considering that the LZ, with olivine Fo_{45}, is only slightly less evolved that the MZ cumulates (Fo_{41} at the base), the melt in equilibrium with LZ, i.e. the FLI parental magma, was slightly more primitive, but still close to a monzonitic composition. How and where can such melt be generated?

A first scenario must be considered. In an anorthosite environment, monzonitic (mangeritic) magmas have been shown to result from fractional crystallization of jotunitic magmas (Wilmart et al., 1989; Vander Auwera et al., 1998b). So it is tempting to invoke this hypothesis. The FLI parental magma would have been discharged from a magma chamber where it was residual melt from fractional crystallization of jotunite. A quasi-equivalent of this magma chamber could have been the Bjerkreim-Sokndal intrusion, where the total thickness of cumulates less evolved than the Transition Zone cumulates is broadly 6300 m, and the Transition Zone itself is ca. 130 m (see Fig. 2 of Wilson et al., 1996). The entire thickness of FLI (320 m) would thus need some 16 km of less evolved cumulates to be accounted for, assuming a magma chamber of relative dimensions comparable to the Bjerkreim-Sokndal intrusion. We have little evidence to support the occurrence of such a thick layered series, although this hypothesis is not completely unrealistic in view of the geophysically plausible existence of gabbroic rocks below the Korosten Pluton, extending down to the base of the crust (Bogdanova et al., 2004).

A second, more simple scenario is preferred here. The FLI monzonitic melt would result from the crystallization of the enclosing Volodarsk-Volynskyy anorthosite massif itself. The intercumulus liquid of the anorthosite would have filtered out of the plagioclase-rich mush and been collected in the FLI magma chamber. The iron-rich nature of interstitial olivine (Fo_{44}) in the enclosing anorthosite indeed indicates that, at least locally, the intercumulus liquid could have

reached evolved compositions. Local occurrence of granophyric pods in the anorthosite also corroborates this hypothesis. Further investigation as to the nature of the gabbros which rim the Volodarsk-Volynskyy massif (Fig. 1) might provide complementary constraints for this model (work in progress).

7. Conclusions

1. The FLI has been divided into a series of lithostratigraphic units, LZ, MZ, UBZ_2 and UBZ_1, which define a trough-shaped internal structure of the intrusion.
2. The dominant mineral assemblage (plagioclase, iron-rich olivine, augite, ilmenite, Ti-magnetite, apatite) is relatively evolved and comparable to that of the upper part of the Skaergaard intrusion and to the Transition Zone of the Bjerkreim-Sokndal layered intrusion.
3. The rocks show typical cumulate textures with conspicuous mineral lamination and have clearly been affected by postcumulus processes, involving the crystallization of trapped liquid and/or grain boundary readjustment.
4. The LZ and MZ result from a continuous fractional crystallization process, clearly evidenced by cryptic layering and trace element variation in whole-rock and mineral compositions. The UBZ displays a reverse evolution, as a result of crystallization downwards from the roof.
5. The chemical compositions of UBZ_1 and LZ cumulates are affected by crystallization of the intercumulus melt, with a proportion decreasing from the margins to the center of the intrusion. The trapped liquid fraction is however lower in the LZ compared to the UBZ_1, probably due to compaction of the cumulate pile at the base of the intrusion and the buoyant behaviour of the monzonitic trapped liquid.
6. Application of the pyroxene QUIlF equilibria confirms that, olivine and Ti-magnetite liquidus compositions have not been significantly modified, particularly where ulvöspinel has been preserved. In these samples subsolidus re-equilibration has been entirely restricted to ilmenite. This allows determination of the fO_2 conditions at liquidus temperatures. Values obtained indicate a variation of ΔFMQ from 0.7 down to −1.4 log units. In other samples, particularly from LZ and UBZ_1, magnetite is completely oxidized in a trellis or sandwich microtexture and shows evidence of inter-oxide reaction. Low fO_2 conditions are also confirmed by the late crystallization of magnetite in the sequence of rocks, and the high V^{3+}-content in the melt, reflected by the high V-content of magnetite (up to 1.85% V). External granule exsolution of ilmenite may have increased the V-content of the oxidized magnetite.
7. Crystal sorting of mafic minerals appears to have played a very minor role in the formation of the MZ cumulates. The major factor controlling the modal composition of the rocks is the plagioclase content. The bulk composition of the MZ rocks can be defined as a first approximation by mixing various proportions of a plagioclase pole with a mafic pole. The straight line joining the two poles contains the locus of the cotectic composition of the MZ cumulates.
8. The composition of a cumulate (C3) in equilibrium with a monzonitic (mangeritic) melt belonging to the jotunitic liquid line of descent also lies on this straight line. We consider that this is not coincidental and that this cumulate is essentially identical to the MZ cotectic assemblage. This cumulate/melt equilibrium relationship being firmly assessed by mass balance modelling and experiments, we infer a similar relationship between the MZ cotectic assemblage and a monzonitic melt. The silica-rich (57% SiO_2) nature of this melt is in agreement with the conclusions of Hunter and Sparks (1987) concerning the Skaergaard liquid line of descent.
9. The FLI parental magma was most probably a residual liquid from crystallization of the enclosing Volodark-Volinskyy anorthosite, rather than a melt discharged from a huge deeper-seated magma chamber, larger than the Bjerkreim-Sokndal layered intrusion.

Acknowledgements

LS has been supported by a GEODE grant and by a NATO scientific research fellowship at the University of Liège. G. Bologne (CIGI, University of Liège) and J. Wauthier (CAMST, Catholic University of Louvain) are greatly thanked for their help with chemical analyses. A. M. Fransolet has kindly identified ulvöspinel by XRD. J. Vander Auwera has discussed many aspects of this work. R. Wilson is greatly thanked for many suggestions that have improved an earlier version of the manuscript. The comments of Wendy Bohrson and of an anonymous reviewer are warmly acknowledged. The Belgian FNRS has supported part of the analytical expenses. BC has benefited from a grant from the Fund for Research in Industry and Agriculture.

Appendix A. Methodology and methods

Whole-rock analyses were performed by XRF on an ARL 9400 XP spectrometer. The major elements, V, Cr and

Ba were analysed on lithium tetra- and metaborate glass discs (FLUORE-X65®), with matrix corrections following the Traill-Lachance algorithm. Trace elements (Sr, Rb, Nb, Zr, Y, Ni, Zn, Co and Cu) were measured on pressed pellets and corrected for matrix effects by Compton peak monitoring. Fe^{2+} was determined by titration.

Selected samples were analysed for REE, U, Th, Hf, Ta and Ga by ICP-MS on a VG Elemental Plasma Quad PQ2 after alkali fusion following the method described in Vander Auwera et al. (1998a).

Ten samples were studied by microprobe analysis (CAMECA SX50). Accelerating voltage was set at 15 kV and elements were counted for 20 s (Ca, K, Ti), 30 s (Si, Al, Fe, Mg, Mn) or 45 s (Na). A combination of synthetic and natural standards was used, and X-ray intensities were reduced using the CAMECA PAP correction program. A defocused beam was used to analyse cloth-textured magnetite.

Some minerals from the same samples were separated and analysed for trace elements. The rocks were crushed to 100–150 μm, separated into two fractions by bromoform, and each fraction was then run through a Frantz magnetic separator at increasing intensities (Duchesne, 1966). Concentrates of magnetite and ilmenite were then purified by centrifugation in hot Clerici solution at densities of 4.8 gcm^{-3} and 4.5 gcm^{-3}, respectively. Concentrates of apatite were purified by centrifugation in bromoform and methylene iodide.

XRF on pressed pellets was used to analyse separated fractions of plagioclase for Sr, of ilmenite for V, Cr, Mn, Ni, Zn, Zr and Nb, and of magnetite for Ti, V, Cr, Zn, and Ni. XRF on Li-tetraborate glass disc was also used to analyse Fe, Ti, Si, Mg, Mn, Al, and Ca in separated ilmenites and magnetites. International references materials (SARM 59 and 12, IGS 31 and 32, GBW 07226), samples 16716 G/91, V4-1, 16717 provided by Titania A/S, as well as synthetic standards and in-house standards, measured by other methods, were used for calibration.

REE in apatite were measured by ICP-MS after differential open acid digestion. Synthetic solutions were used for calibration.

Appendix B. Supplementary data

Supplementary data associated with this article can be found, in the online version, at doi:10.1016/j.lithos.2006.01.003.

References

Amelin, Y.V., Heaman, L.M., Verkhogliad, V.M., Skobelev, V.M., 1994. Geochronological constraints on the emplacement history of an anorthosite-rapakivi granite suite: U–Pb zircon and baddeleyite study of the Korosten complex, Ukraine. Contrib. Mineral. Petrol. 116, 411–419.

Andersen, D.J., Lindsley, D.H., Davidson, P.M., 1993. QUILF: a Pascal program to assess equilibria among Fe–Mg–Ti oxides, pyroxenes, olivine, and quartz. Comput. Geosci. 19, 1333–1350.

Ashwal, L.D., 1993. Anorthosites. Springer, Berlin, Heidelberg. 422 pp.

Barnes, S.J., 1986. The effect of trapped liquid crystallization on cumulus mineral composition in layered intrusions. Contrib. Mineral. Petrol. 93, 523–531.

Bogdanova, S., et al., 2004. The 1.80–1.74 Ga anorthosite-rapakivi granite Korosten Pluton in the Ukrainian Shield: a 3-D geophysical reconstruction of deep structure. Tectonophysics 381, 5–27.

Cawthorn, R.G., 1996. Layered igneous rocks. Development in Petrology. Elsevier, Amsterdam. 531 pp.

Cawthorn, R.G., Molyneux, T.G., 1986. Vanadiferous magnetite deposits of the Bushveld Complex. In: Anhaeusser, C.R., Maske, S. (Eds.), Mineral Deposits of Southern Africa. Geol Soc S Afr, pp. 1251–1266.

Charlier, B., Vander Auwera, J., Duchesne, J.C., 2005. Geochemistry of cumulates from the Bjerkreim-Sokndal layered intrusion (S. Norway): Part II. REE and the trapped liquid fraction. Lithos 83, 255–276.

Demaiffe, D., Hertogen, J., 1981. Rare earth element geochemistry and strontium isotopic composition of a massif-type anorthositic–charnockitic body: the Hidra massif (Rogaland, SW. Norway). Geochim. Cosmochim. Acta 45, 1545–1561.

Duchesne, J.C., 1966. Séparation rapide des minéraux des roches. Ann. Soc. Géol. Belg. 69, 347–356.

Duchesne, J.C., 1970. Microstructures of Fe–Ti oxide minerals in the South Rogaland anorthositic complex (Norway). Ann. Soc. Géol. Belg. 93, 527–544.

Duchesne, J.C., 1972. Iron–titanium oxide minerals in the Bjerkrem-Sogndal massif, South-Western Norway. J. Petrol. 13, 57–81.

Duchesne, J.C., 1990. Origin and evolution of monzonorites related to anorthosites. Schweiz. Mineral. Petrogr. Mitt. 70, 189–198.

Duchesne, J.C., 1996. Liquid ilmenite or liquidus ilmenite: a comment on the nature of ilmenite vein deposit. In: Demaiffe, D. (Ed.), Petrology and Geochemistry of Magmatic Suites of Rocks in the Continental and Oceanic Crusts. ULB-MRAC, Bruxelles, pp. 73–82.

Duchesne, J.C., 1999. Fe–Ti deposits in Rogaland anorthosites (South Norway): geochemical characteristics and problems of interpretation. Miner. Depos. 34, 182–198.

Duchesne, J.C., Charlier, B., 2005. Geochemistry of cumulates from the Bjerkreim-Sokndal layered intrusion (S. Norway): Part I. Constraints from major elements on the mechanism of cumulate formation and on the jotunite liquid line of descent. Lithos 83, 229–254.

Duchesne, J.C., Hertogen, J., 1988. Le magma parental du lopolithe de Bjerkreim-Sokndal (Norvège méridionale). C. R. Acad. Sci. Paris 306, 45–48.

Duchesne, J.C., Korneliussen, A., (Eds.), 2003. Ilmenite deposits and their geological environment, with special reference to the Rogaland Anorthosite Province, including a geological map at scale 1:75,000 and a CD with a guide to the province. NGU Special publication 9. Geological Survey of Norway. 138 pp.

Duchesne, J.C., Demaiffe, D., Roelandts, I., Weis, D., 1985. Petrogenesis of monzonoritic dykes in the Egersund-Ogna anorthosite (Rogaland, S.W. Norway): trace elements and isotopic constraints. Contrib. Mineral. Petrol. 90, 214–225.

Duchesne, J.C., Denoiseux, B., Hertogen, J., 1987. The norite–mangerite relationships in the Bjerkreim-Sokndal layered lopolith (SW Norway). Lithos 20, 1–17.

Duchesne, J.C., Wilmart, E., Demaiffe, D., Hertogen, J., 1989. Monzonorites from Rogaland (Southwest Norway): a series of rocks coeval but not comagmatic with massif-type anorthosites. Precambrian Res. 45, 111–128.

Duchesne, J.C., Liégeois, J.P., Vander Auwera, J., Longhi, J., 1999. The crustal tongue melting model and the origin of massive anorthosites. Terra Nova 11, 100–105.

Emslie, R.F., 1985. Proterozoic anorthosite massifs. In: Tobi, A.C., Touret, J.L.R. (Eds.), The Deep Proterozoic Crust in the North Atlantic Provinces. NATO Adv. Stud. Inst., vol. C158. Reidel, Dordrecht, pp. 39–60.

Ford, C.E., Russell, D.G., Craven, J.A., Fisk, M.R., 1983. Olivine–liquid equilibria: temperature, pressure and composition dependence on the crystal/liquid cation partition coefficients for Mg, Fe^{2+}, Ca and Mn. J. Petrol. 24, 256–265.

Frost, B.R., Lindsley, D.H., 1992. Equilibria among Fe–Ti oxides, pyroxenes, olivine, and quartz: Part II. Application. Am. J. Sci. 77, 1004–1020.

Frost, B.R., Lindsley, D.H., Andersen, D.J., 1988. Fe–Ti oxide-silicate equilibria: assemblages with fayalitic olivine. Am. Mineral. 73, 727–740.

Grove, T.L., Baker, M.B., Kinzler, R.J., 1981. Coupled CaAl–NaSi diffusion in plagioclase feldspar: experiments and application to cooling rate speedometry. Geochim. Cosmochim. Acta 58, 2113–2121.

Gursky, D., Nechaev, S., Bobrov, A., 2003. Titanium deposits in Ukraine focussed on the Proterozoic anorthosite-hosted massifs. In: Duchesne, J.C., Korneliussen, A. (Eds.), Ilmenite Deposits and their Geological Environment. NGU Special Publication, vol. 9. Geological Survey of Norway, pp. 21–26.

Hoover, J.D., 1989. The chilled Marginal Gabbro and other contact rocks of the Skaergaard intrusion. J. Petrol. 30, 441–476.

Hunter, R.H., 1996. Texture development in cumulate rocks. In: Cawthorn, R.G. (Ed.), Layered Intrusions. Elsevier, pp. 77–101.

Hunter, A., Sparks, R.S.J., 1987. The differentiation of the Skaergaard Intrusion. Contrib. Mineral. Petrol. 95, 451–461.

Jang, Y.D., Naslund, H.R., McBirney, A.R., 2001. The differentiation of the Skaergaard intrusion and the timing of magnetite crystallization: iron enrichment revisited. Earth Planet. Sci. Lett. 189, 189–196.

Jensen, J.C., Nielsen, F.M., Duchesne, J.C., Demaiffe, D., Wilson, J.R., 1993. Magma influx and mixing in the Bjerkreim-Sokndal layered intrusion, South Norway: evidence from the boundary between two megacyclic units at Storeknuten. Lithos 29, 311–325.

Kilinc, A., Carmichael, I.S.E., Rivers, M.L., Sack, R.O., 1983. The ferric–ferrous ratio of natural silicate liquids equilibrated in air. Contrib. Mineral. Petrol. 83, 136–140.

Lindsley, R.F., Frost, B.R., 1992. Equilibria among Fe–Ti oxides, pyroxenes, olivine, and quartz: Part I. Theory. Am. Mineral. 77, 987–1003.

Longhi, J., 2005. A mantle of mafic crustal source for Proterozoic anorthosites. Lithos 83, 183–198.

Longhi, J., Vander Auwera, J., Fram, M., Duchesne, J.C., 1999. Some phase equilibrium constraints on the origin of Proterozoic (Massif) anorthosites and related rocks. J. Petrol. 40, 339–362.

McBirney, A.R., 1975. Differentiation of the Skaergaard intrusion. Nature 253, 691–694.

McBirney, A.R., 1996. The Skaergaard intrusion. In: Cawthorn, R.G. (Ed.), Layered Intrusions. Elsevier, Amsterdam, pp. 147–180.

McBirney, A.R., Naslund, H.R., 1990. The differentiation of the Skaergaard intrusion. A discussion of Hunter and Sparks (Contrib Mineral Petrol 95:451–461). Contrib. Mineral. Petrol. 104, 235–247.

McCallum, I.S., 1996. The stillwater complex. In: Cawthorn, R.G. (Ed.), Layered Intrusions. Elsevier, Amsterdam, pp. 441–484.

Michot, J., Michot, P., 1969. The problem of anorthosites: the South Rogaland igneous complex, southern Norway. In: Isachsen, Y.W. (Ed.), Origin of Anorthosite and Related Rocks. New York State Museum Sciences Service Mem, pp. 399–410.

Mitrokhin, A.V., 2003. The gabbro-anorthosite massifs of Korosten Pluton (Ukraine) and problems concerning the evolution of the parental magmas. In: Duchesne, J.C., Korneliussen, A. (Eds.), Ilmenite deposits and their geological environment. NGU Special Publication, vol. 9. Geological Survey of Norway, pp. 96–97.

Morse, S.A., 1982. A partisan review of Proterozoic anorthosites. Am. Mineral. 67, 1087–1100.

Morse, S.A., 1990. A discussion of Hunter and Sparks (Contrib Mineral Petrol 95:451–461). Contrib. Mineral. Petrol. 104, 240–244.

Morse, S.A., Lindsley, D.H., Williams, R.J., 1980. Concerning intensive parameters in the Skaergaard intrusion. Am. J. Sci. 280, 159–170.

Owens, B.E., Rockow, M.W., Icenhower, J.P., Dymek, R.F., 1993. Jotunites from the Grenville Province, Quebec: petrological characteristics and implications for massif anorthosite petrogenesis. Lithos 30, 57–80.

Parsons, I. (Ed.), 1987. Origins of igneous layering. NATO Adv. Stud. Inst. Series, vol. C196. Reidel, Dordrecht. 666 pp.

Prykhodko, V.L., et al., 2002. Fedorivske apatite–ilmenite deposit. Main Types of Rock Complexes and Mineral Deposits in the Ukrainian Shield, Geological Excursion Guidebook. Geographica, Kyiv. 35–38 pp.

Ramdohr, P., 1953. Ulvöspinel and its significance in titaniferous iron ores. Econ. Geol. 48, 677–688.

Roeder, P.L., Emslie, R.F., 1970. Olivine–liquid equilibrium. Contrib. Mineral. Petrol. 19, 275–289.

Scoates, J.S., Frost, C.D., Mitchell, J.N., Lindsley, D.H., Frost, B.R., 1996. Residual-liquid origin for a monzonoritic intrusion in a mid-Proterozoic anorthosite complex: the Sybille intrusion, Laramie anorthosite complex, Wyoming. Geol. Soc. Amer. Bull. 108, 1357–1371.

Shcherbak, N.P., Volodin, D.F., (Eds.), 1984. Geological map of the Precambrian rocks of the Ukrainian Shield, Scale 1:1000000, one sheet. Ministry of Geology, UkSSR, Kiev.

Skobelev, V.M., 1987. Geochemistry and Geochronology of Precambrian of the North-Western region of the Ukrainian Shield (in Russian). Naukova Dumka, Kyiv.

Snyder, D., Carmichael, I.S.E., Wiebe, R.A., 1993. Experimental study of liquid evolution in a Fe-rich, layered mafic intrusion: constraints of Fe–Ti oxide precipitation on the T–fO_2 and T–ρ path of tholeiitic magmas. Contrib. Mineral. Petrol. 113, 73–86.

Spencer, K.J., Lindsley, D.H., 1966. A solution model for coexisting iron–titanium oxides. Am. Mineral. 66, 1189–1201.

Sun, S.S., McDonough, W.F., 1989. Chemical and isotopic systematics of oceanic basalts: implications for mantle composition and processes. In: Saunders, A.D., Norry, M.J. (Eds.), Magmatism in Ocean Basins. Geol. Soc. London Spec. Pub, pp. 313–345.

Taylor, S.R., Campbell, I.H., McCulloch, M.T., McLennan, S.M., 1984. A lower crustal origin for massif-type anorthosites. Nature 311, 372–374.

Tegner, C., 1997. Iron in plagioclase as a monitor of the differentiation of the Skaergaard intrusion. Contrib. Mineral. Petrol. 128, 45–51.

Thy, P., 1982. Titanomagnetite and ilmenite in the Fongen-Hyllingen basic complex, Norway. Lithos 15, 1–16.

Toplis, M., Carroll, M.R., 1994. An experimental study of the influence of oxygen fugacity on Fe–Ti oxide stability, phase relations, and mineral-melt equilibria in ferro-basaltic systems. J. Petrol. 36, 1137–1170.

Toplis, M., Corgne, A., 2002. An experimental study of element partitioning between magnetite, clinopyroxene and iron-bearing silicate liquids with particular emphasis on vanadium. Contrib. Mineral. Petrol. 144, 22–37.

Toplis, M., Dingwell, D.B., Libourel, G., 1994a. The effect of phosphorus on the iron redox ratio, and density of an evolved ferro-basalt. Contrib. Mineral. Petrol. 117, 293–304.

Toplis, M., Libourel, G., Carroll, M.R., 1994b. The role of phosphorus in crystallisation processes of basalt: an experimental study. Geochim. Cosmochim. Acta 58, 797–810.

Vander Auwera, J., Bologne, G., Roelandts, I., Duchesne, J.C., 1998a. Inductively coupled plasma-mass spectrometry (ICP-MS) analysis of silicate rocks and minerals. Geol. Belg. 1, 49–53.

Vander Auwera, J., Longhi, J., Duchesne, J.C., 1998b. A liquid line of descent of the jotunite (hypersthene monzodiorite) suite. J. Petrol. 39, 439–468.

Verkhogliad, V.M., 1995. Age stages of Korosten pluton magmatism (in Russian). Geochem. Ore Form. 21, 34–47.

Vernon, R.H., 2004. A Practical Guide to Rock Microstructure. Cambridge University Press, Cambridge. 594 pp.

Vincent, E.A., 1960. Ulvöspinel in the Skaergaard intrusion, Greenland. Neues Jahrb. Mineral. Abh. (Festband Ramdohr) 94, 993–1016.

Vincent, E.A., Phillips, R., 1954. Iron–titanium oxide minerals in layered gabbros of the Skaergaard intrusion, East Greenland. Geochim. Cosmochim. Acta 6, 1–26.

Wager, L.R., Brown, G.M., 1968. Layered Igneous Rocks. Oliver and Boyd, London. 588 pp.

Wiebe, R.A., 1992. Proterozoic anorthosite complexes. In: Condie, K. C. (Ed.), Proterozoic Crustal Evolution. Development in Precambrian Research, vol. 10. Elsevier, Amsterdam, pp. 215–262.

Wilmart, E., Clocchiatti, R., Duchesne, J.C., Touret, J.L.R., 1991. Fluid inclusions in charnockitic rocks from the Bjerkreim-Sokndal massif (Rogaland, Southwestern Norway): fluid origin and in situ evolution. Contrib. Mineral. Petrol. 108, 453–468.

Wilmart, E., Demaiffe, D., Duchesne, J.C., 1989. Geochemical constraints on the genesis of the Tellnes ilmenite deposit (S.W. Norway). Econ. Geol. 84, 1047–1056.

Wilson, J.R., Robins, B., Nielsen, F., Duchesne, J.C., Vander Auwera, J., 1996. The Bjerkreim-Sokndal layered intrusion, Southwest Norway. In: Cawthorn, R.G. (Ed.), Layered Intrusions. Elsevier, Amsterdam, pp. 231–256.

Zack, T., Brumm, R., 1998. Ilmenite/liquid partition coefficients of 26 trace elements determined through ilmenite/clinopyroxene partitioning in garnet pyroxene. In: Gurney, J., Gurney, J.L., Pascoe, M. D., Richardson, S.H. (Eds.), 7th International Kimberlite Conference. Red Roof Design, Cape Town.